Run-09 pC Analysis

...

Contents

1. Introduction

In this analysis we discuss the analysis of RHIC run 2009 pC data (February – July 2009). The pC measurements were performed for 250 GeV beams (February – April) and for 100 GeV beams (April – July). Analysis apporach is basically very similar to one developed for 2005 pC data analysis [1] and also used for 2006 and 2008 data analysis [2], and includes the following steps:

- Energy calibration with alpha source

- Determination of energy and time corrections, for each measurement (run)

- QA analysis to mask bad strips, for each measurement (run)

- QA analysis to reject bad measurements (runs)

- Normalization of pC measurements to HJet absolute polarization measurements.

- Evaluation of systematic uncertainties for polarization measurements

Before 2009 RHIC Run the pC polarimeter system was upgraded, so that we had two polarimeters in each ring, with their own target and detector systems, and which shared the same DAQ system (shapers, WFDs). It allowed us not only to perform measurements of both vertical and horizontal polarization profiles every time the pC polarization measurement is done during RHIC store, and test new detectors, but also to provide a very important cross check for our results by comparing the measurements obtained by two polarimeters, in each ring. In the following we call polarimeters Blue1 and Blue2 (Blue2 is upstream) in blue ring and Yellow1 and Yellow2 (Yellow1 is upstream) in yellow ring.

In each polarimeter, carbon targets were installed on two target ladders, one with six horizontal targets and another one with six vertical targets. Two identical target mortion mechanisms were used to perform measurements either with vertical or horizontal target.

Detector system in each polarimeter to detect recoil carbon consisted of 6 Silicon strip detectors (numbered from 0 to 5 in the following) mounted in a vacuum chamber at azimuthal angles of 90 (detectors 1 and 4) and ±45 degrees (detectors 0, 2, 3 and 5) relative to vertical direction (the stable proton spin direction at RHIC). Each of the detectors was segemented into 12 srtrips (so 72 strips numbered from 0 to 71 in the following). All detectors except 90 degree detectors in Blue2 and Yellow2 were identical ones manufactured by the BNL's Instrumentation Division. The Hamamatsu strip photodiods (also segmented into 12 strips) were instaled in 90 degree detector slots in Blue2. The Hamamatsu single photodiods (two pairs) were installed in 90 degree slots in Yellow2, which had their own (slow) DAQ system and were not used in the current analysis.

In Run9 we experienced serious systematic problems in pC measurements related to high event rates (a factor 2-3 higher than in previous years), which mainly come from thinner transverse beam size (higher luminosity) for 250 GeV beams and on the average thicker targets used for the measurements. It will be discussed in more details below in this note.

Since 2008 the main pC operational mode is target scan: during the measurement target was moving across the beam with uniform spead. This allowed us to measure not only the

average polarization across the beam, but also polarization profile and intensity profile (beam emittance). Sometimes measurements were done in fixed target mode: target was placed at beam maximum intenity. In this analysis we used only scan measurements.

pC polarization measurements in physics fills of Run9 were organized in such a way that if for example Polarimter-1 was used for horizontal scan (with vertical target), Polarimeter-2 was used for vertical scan (with horizontal target). If a measurement is done with horizontal target 90 degree detectors (detectors 1 and 4) are partially shadowed, so they didn't participate in polarization measurements.

Fig. 1 and 2 summarizes information on targets used in Run9 measurements.

In all plots in this note only statistical errors are shown unless mentioned otherwise.

2. Response to alphas, energy calibration

The energy calibration of detectors is performed using ^{241}Am α source with energy spectrum containing two major lines 5.486 MeV (85%) and 5.443 MeV (13%), which are undistingushable in our measurements. Since the kinetic energy of α is more than a factor of 5 higher than the maximal carbon energy used for regular polarization measurements, the signal output for the alpha calibration runs was ×5 attenuated.

Dedicated calibration runs were performed several times throughout Run9 to monitor gain drift and operability of strips. Fig. 3 shows the typical result from calibration run. Alpha peaks show up at about 180 counts in all strips. Two edge strips in detector 1 and 6 (strips 0, 1 and 70, 71) were shadowed so were not well exposed to alphas. The calibration coefficient for them was assigned from the average over 10 good strips in the corresponding detector. Slightly lower response (at ∼150 counts) was observed in Hamamatsu strip photodiods in 90 degree detectors of Blue2.

The strip by strip gain drift in each polarimeter was monitored by the comparison of alpha peaks measured in different calibration runs. Fig. 4 shows the typical example of the strip-by-strip comparison of alpha peaks measured in Blue1 detectors on April 29 and July 6. This particular example shows the average shift of about 0.3%. Only strip 33 (in detector 2) showed abnomal behavior in Blue1, so was excluded from the analysis.

Fig. 5 and 6 shows the summary of alpha peak variation in all calibration runs in Run9. Red points and error bars represent Mean and RMS values, and blue points and error bars represent mean and sigma from gaussian fit of the distribution of the strip-by-strip relative shift, as for example on Fig. 4. The points in which red error bars are considerably larger than blue error bars corresponds to the measurements in which one or more strips showed abnomal shift. They are strip 33 in blue1 and blue2 (they correspond to the same WFD channel), and strips 50, 53 and 55 in Yellow1. They were excluded from offline polarization analysis.

Different detectors in a polarimeter behaved in a similar way, as for example is shown in Fig. 7.

As seen on the figures the maximal variation of the average amplitude to α particles didn't exceed 2% throughout Run9, which if not corrected would lead to no more that 2% shift in measured asymmetries. Actually our analysis technique for energy and time correction (from "Dead layer" and T0 fit), to be discussed bellow, partially (by about a half) corrects for the gain shift (attributing the gain shift to the change in effective "Dead
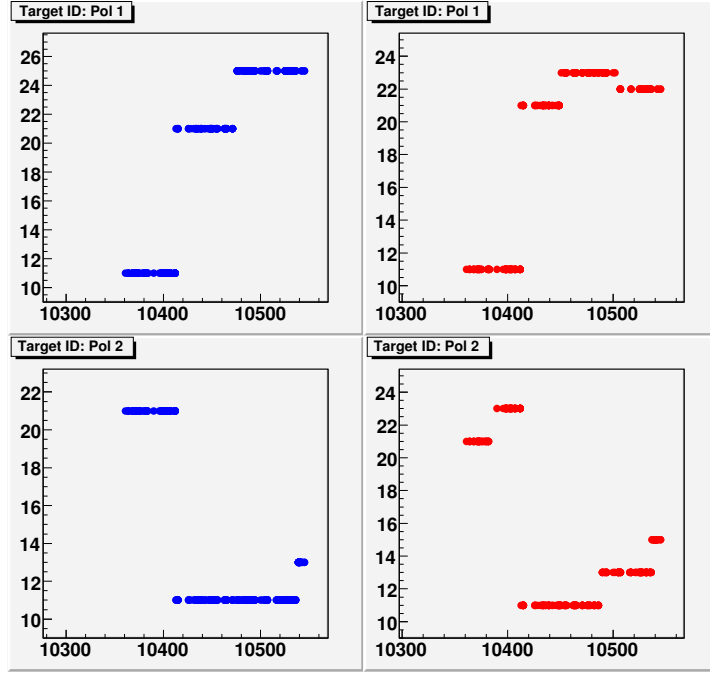
Figure 1. Target ID in $\sqrt{s}$=500 GeV measurements vs fill number (each fill usually had several measurements, all of them are shown here); top left - Blue1, bottom left - Blue2, top right - Yellow1 and bottom right - Yellow2; Target ID is 10+id for vertical targets and 20+id for horizontal targets, where id is target identificator on target ladder (vertical or horizontal).
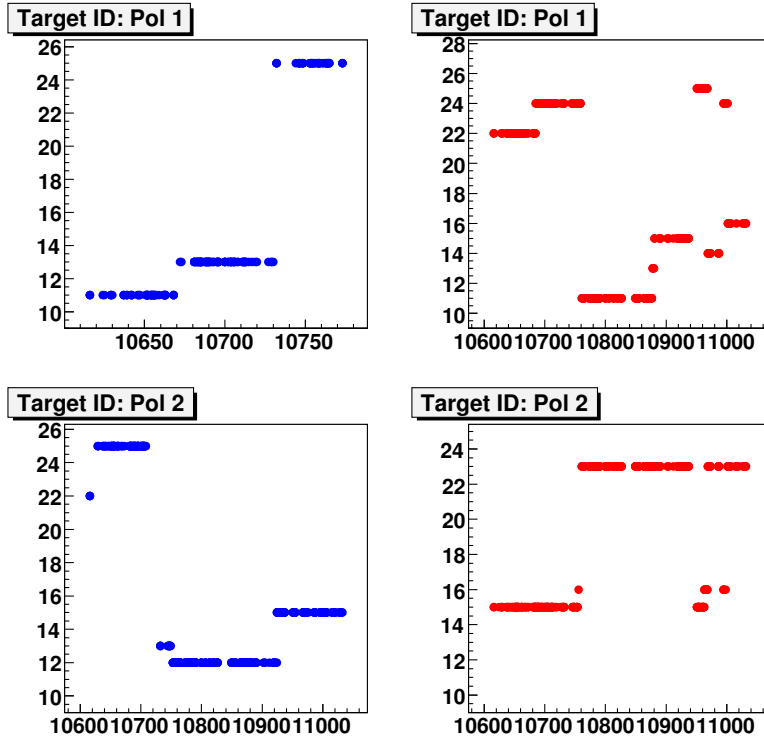

Figure 2. The same as Fig. 1, but for $\sqrt{s}$=200 GeV measurements; notice that Blue1 didn't have measurements in fills >10773.
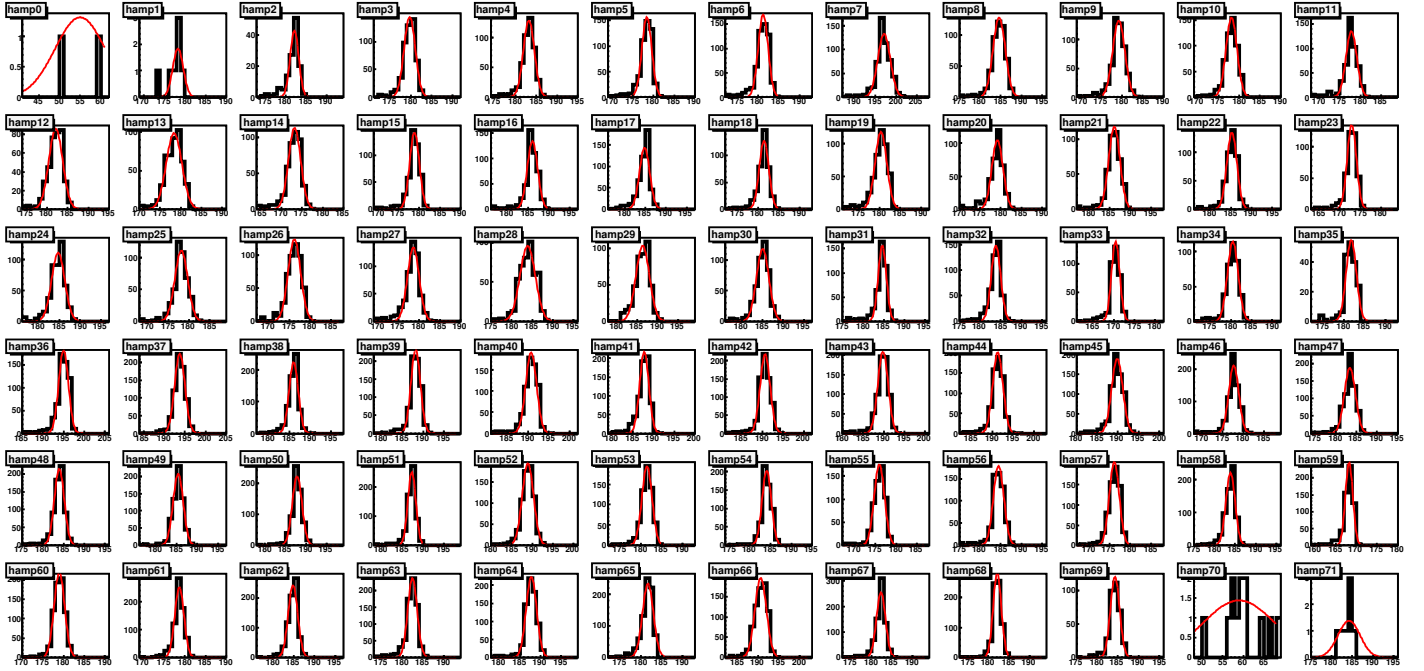
Figure 3. Amplitude response to alphas in April 29 calibration run for Blue1, in each of 72 strips; red lines represent gaussian fit.
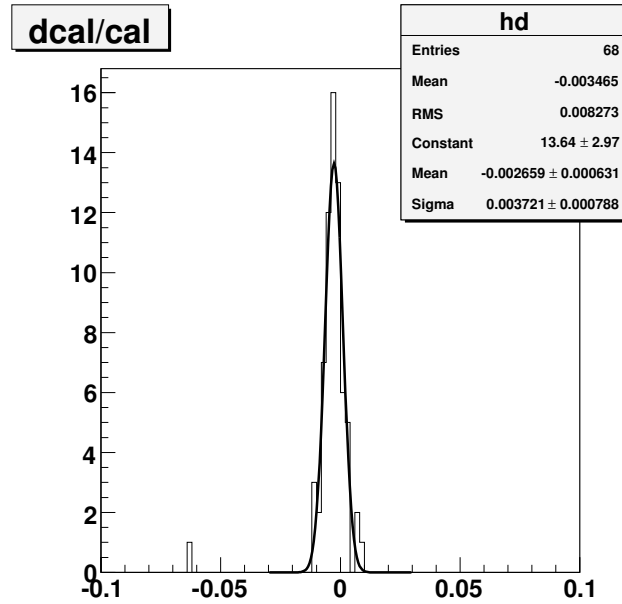

Figure 4. Relative shift in the alpha peak measured in Blue1 strips on July 6 vs April 29. (The outlier on the plot corresponds to strip 33.)
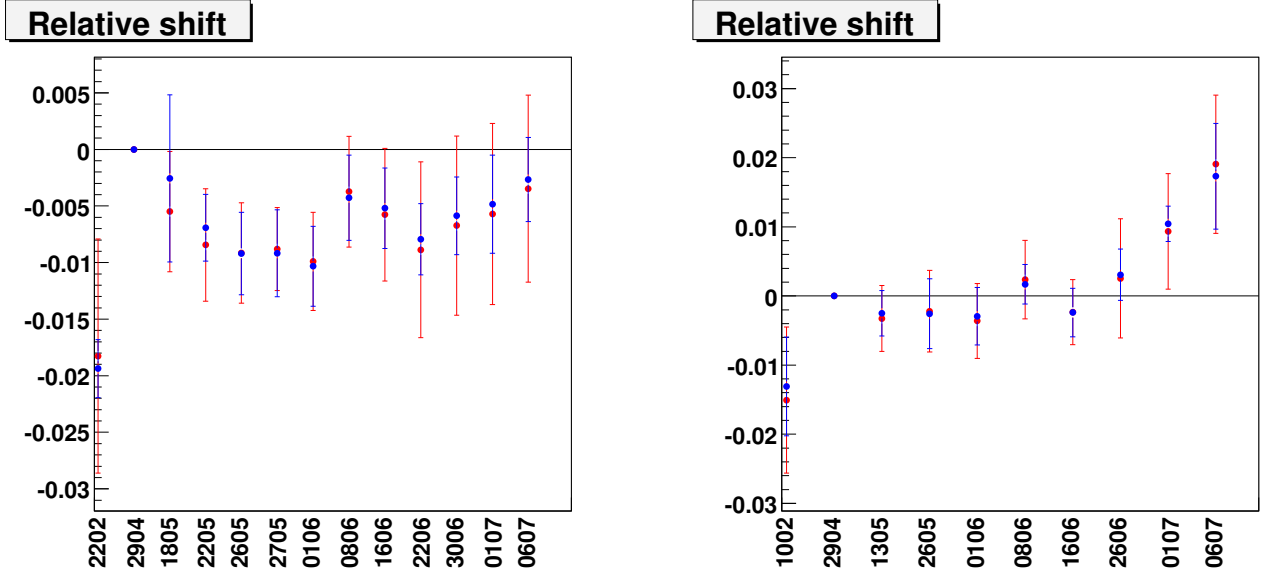
Figure 5. Average over the polarimeter relative variation of alpha peak, left - for Blue1, right - for Blue2, in alpha calibration runs in Run9; results are shown from Feb 22 ("2202" in Blue1) and Feb 10 ("1002" in Blue2) to July 6 ("0607"); relative comparison performed to results from April 29 ("2904"). Red points and error bars represent Mean and RMS values, and blue points and error bars represent mean and sigma from gaussian fit of the distribution of the strip-by-dstrip relative shift, as for example on Fig. 4.
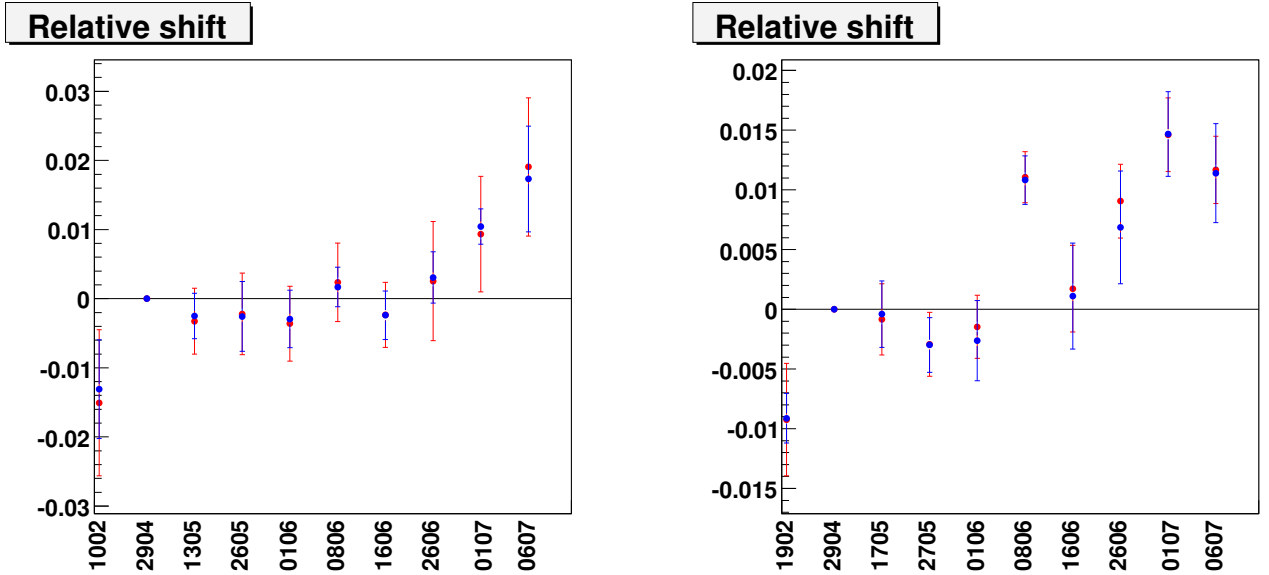

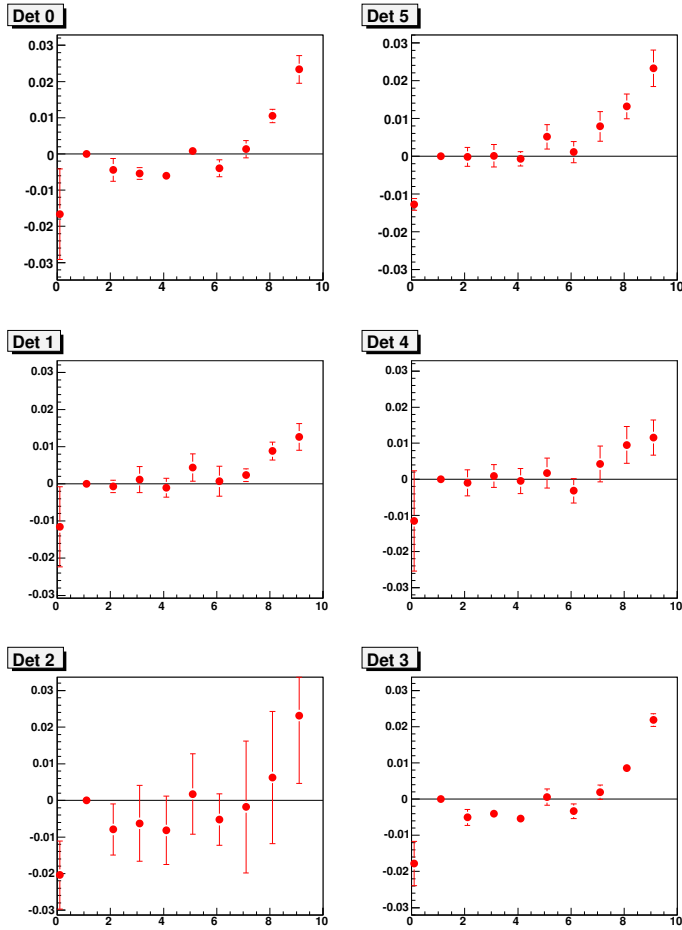Figure 6. The same as on Fig. 5, but for Yellow1 (left) and Yellow2 (right).

Figure 7. Average over a detector relative variation of alpha peak in Blue2; 6 detectors are shown; points and error bars represent Mean and RMS values of the distribution of the strip-by-strip relative shift, as for example on Fig. 4.

layer"), so that the residual effect for polarization measurements will be no more than 1% for 2% shift in gains.

From these quantitative considerations we safely fixed energy calibration coefficients (gains) for the whole Run9.

3. Response to recoil carbons

Fig. 8 shows pC polarimeter typical response to recoil carbon ions - banana-like band in the time of flight vs energy distribution measured by Si detector. Two corrections are necessary here: time of flight offset ($t0$) and correction for the energy loss in Si dead layers to correct carbon deposited energy to kinetic energy. As in previous years analyses these corrections were obtained from the kinematical fit of banana extracting two parameters, $t0$ and effective dead layer x_{DL}:

$$E_{kin} = E_{meas} + E_{loss}(x_{DL}, E) = \frac{1}{2} \cdot M \cdot \frac{L^2}{(t_{meas} + t_0)^2} \tag{1}$$

where M is carbon mass, L is flight path length (distance between target and detector, here $\sim$18 cm), E_{meas} and t_{meas} are measured (depositted) energy and time of flight.

This effective dead layer includes not only the real dead layer but also other effects which lead to the distortion of energy measurements in polarimeter system. In the past, if measurements are performed in good conditions (low event rate, thin uniform target etc.) with newly installed detectors, the extracted from the fit effective dead layer was usually in reasonable agreement with real dead layer of Si detectors calculated from p+ doping layer depth [1,3].

The stability of the energy and time of flight measurements in polarimeter can be monitored by fill or run dependence of reconstructed C mass from measured time of flight t (corrected for t_0) and kinetic energy E_{kin}. Fig. 9 and 10 show the reconstructed mass in 2009 pC measurements. The energy and time of flight corrections (parameters x_{DL} and $t0$ are fixed for all measurements in each polarimeter strip-by-strip at values obtained in the beginning of Run9 (from runs 10328.002, 10346.204, 10328.102 and 10346.306 for Blue1, Blue2, Yellow1 and Yellow2 respectively). These parameters are used for online values throughout Run9.

The variation in reconstructed mass is correlated with event rate, which is measured as the number of carbon events in the banana plot in the E_{kin} range 400–900 keV. The history of event rate per strip in Run9 pC measurements is shown on Fig. 11 and 12. For the comparison, in Run6 (Run8) rates were below 30 kHz (60 kHz) per strip. As it is seen from Fig. 13 and 14 the correlation between reconstructed C mass and rate has several components, meaning that event rate is not the only observable here which affects the reconstructed mass. The reconstructed mass includes two measured values, time of flight and energy, and they can have different dependencies. This will be discussed in the next section.

4. Energy and Time of Flight correction

Similar to previous years analyses [1,2] we performed banana fit to extract parameters $t0$ and x_{DL} as on Fig. 8 in all pC measurements. As it is seen from Fig. 15 and 16, $t0$
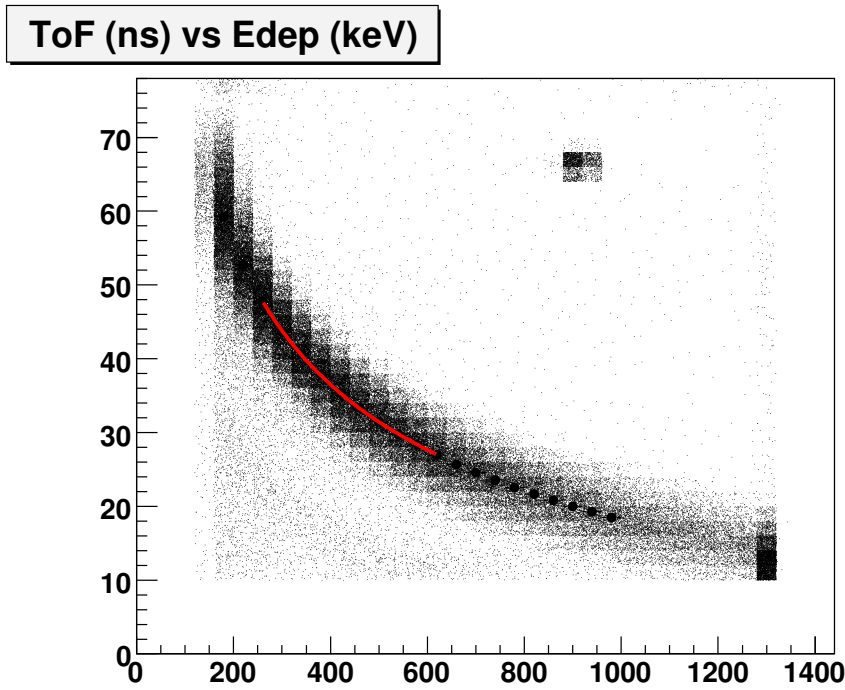
ToF (ns) vs Edep (keV)

Figure 8. Example of pC polarimeter response to Carbon ions ("banana") from run 10765.006 (Blue1), strip 1: ToF vs depositted energy. Red line is a kinematical fit with two free parameters, $t0$ and x_{DL}; the extracted parameter values for this case are $t0$=-21 ns and x_{dl}=63 μg/cm^2; the fitting range in depositted energy roughly corresponds to 400–900 keV range in kinetic energy (after correction of depositted energy due to x_{DL}) - this is the range used for asymmetry (beam polarization) measurements in pC.
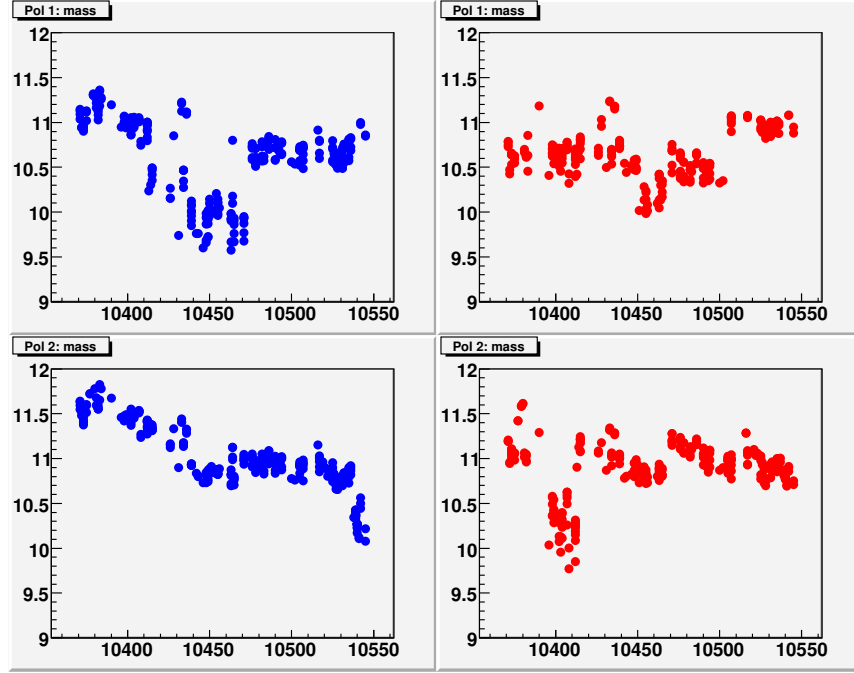
Figure 9. Reconstructed C mass (GeV/c²) in $\sqrt{s}$=500 GeV measurements vs fill number (each fill usually had several measurements, all of them are shown here); top left - Blue1, bottom left - Blue2, top right - Yellow1 and bottom right - Yellow2.
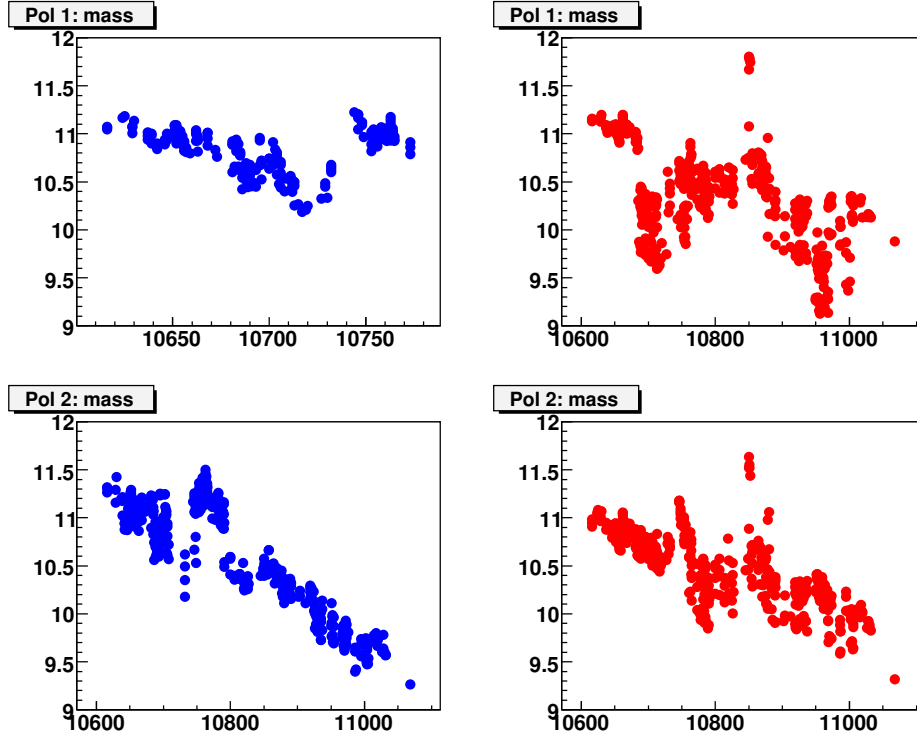

Figure 10. The same as Fig. 9, but for $\sqrt{s}$=200 GeV measurements; notice that Blue1 didn't have measurements in fills >10773.
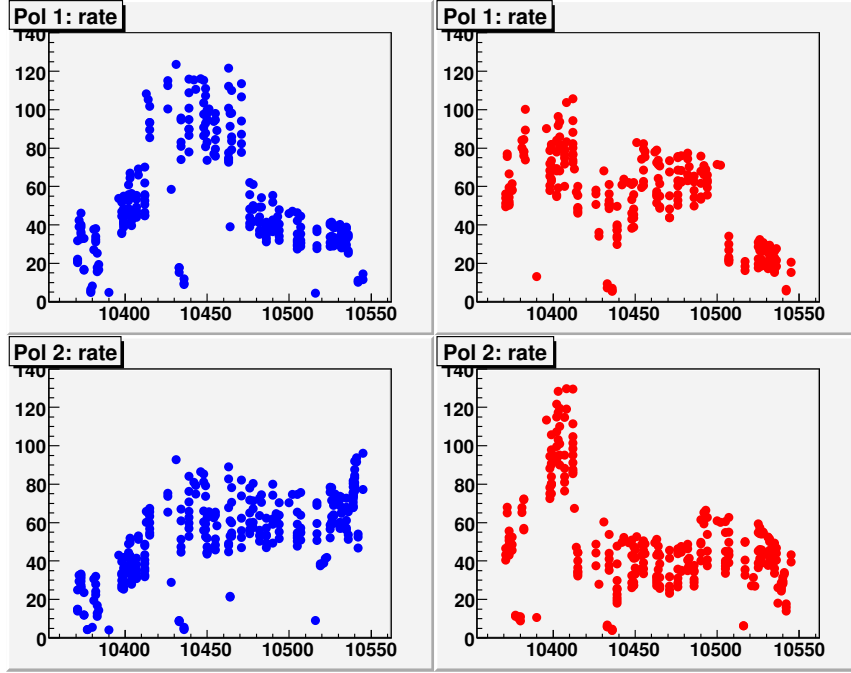
Figure 11. Rate of Carbon events per strip (kHz) in $\sqrt{s}$=500 GeV measurements vs fill number (each fill usually had several measurements, all of them are shown here); top left - Blue1, bottom left - Blue2, top right - Yellow1 and bottom right - Yellow2.
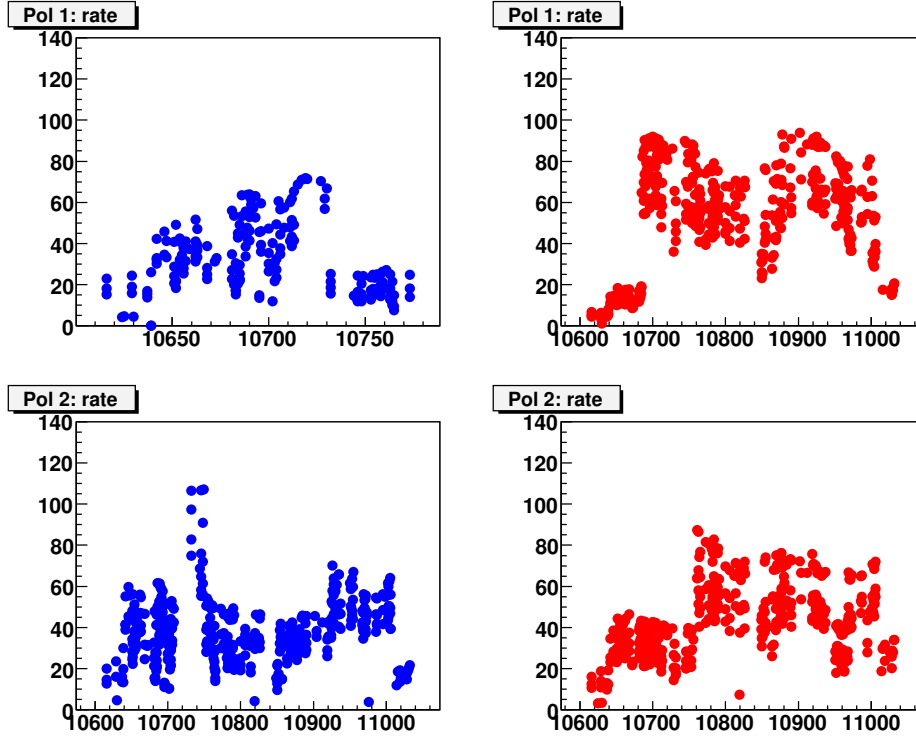

Figure 12. The same as Fig. 11, but for $\sqrt{s}$=200 GeV measurements; notice that Blue1 didn't have measurements in fills >10773.
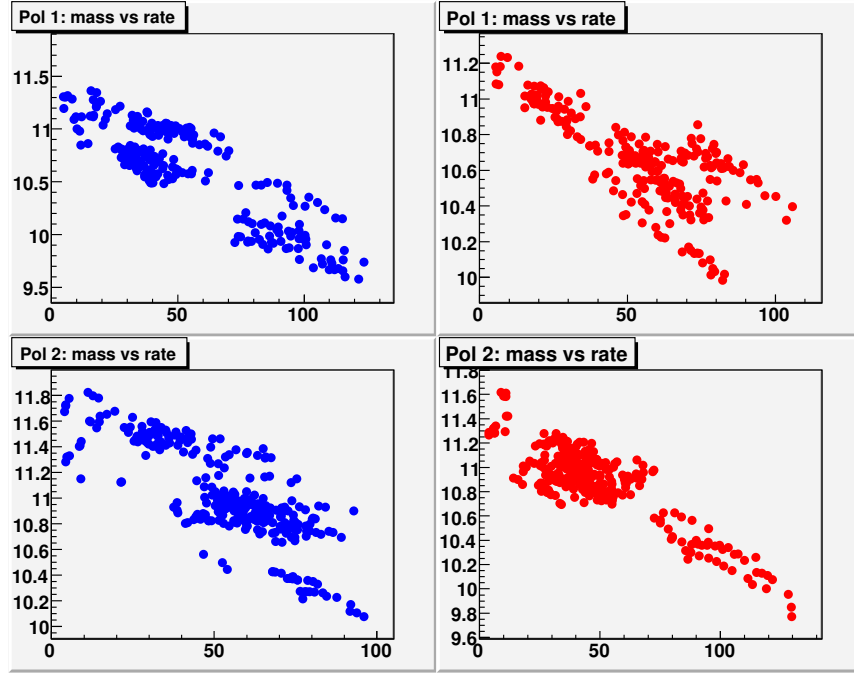
Figure 13. Reconstructed mass (GeV/c²) vs carbon event rate per strip (kHz) in $\sqrt{s}$=500 GeV measurements (each fill usually had several measurements, all of them are shown here); top left - Blue1, bottom left - Blue2, top right - Yellow1 and bottom right - Yellow2.
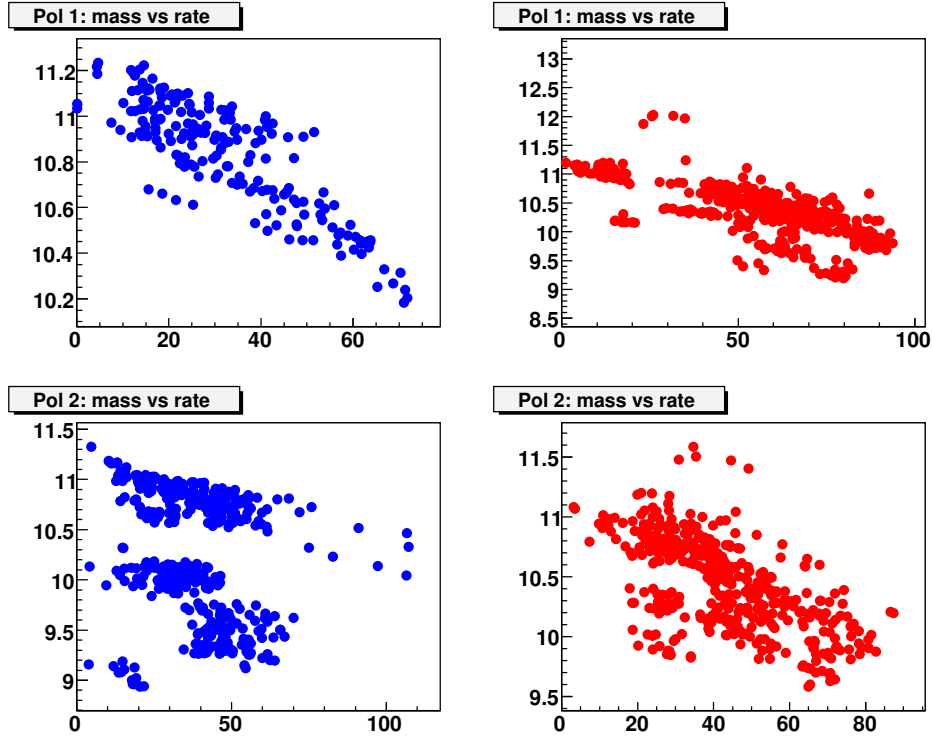

Figure 14. The same as Fig. 13, but for $\sqrt{s}$=200 GeV measurements; notice that Blue1 didn't have measurements in fills >10773.

globally drifted to smaller values, but at different extent: e.g. by less than 1 ns in Yellow1 of $\sqrt{s}$=500 GeV data, and $\sim$5 ns in Blue2 of $\sqrt{s}$=200 GeV data. Similar trend was observed in previous year Spin Runs. The nature of this effect is not yet well understood. Fig. 17 shows that the $t0$ global trend is about the same in all detectors (here in Blue2). Notice that on this Fig. detectors 1 and 4 are Hamamatsu strip photodiods, all others are BNL's Si detectors. So the global effect is approximately not detector dependent.

Also it's worth commenting here that the $t0$ drift can not be just an artifact of the fit. If it were so, it had to be compensated by the shift in energy measurements (x_{DL}) according to Eq. (1). For example, for Blue2 polarimeter, the shift in $t0$ by 5 ns from the beginning to the end of $\sqrt{s}$=200 GeV part of Run9 would correpond to the shift in x_{DL} by $\sim$30 μg/cm^2 or $\sim$20% shift in analysing power (or measured beam polarization). This is not supported by the comparison of Blue2 and HJet measurements (shown later in this note).

The history of x_{DL} is shown on Fig. 18 and 19. Fig. 20 shows that the x_{DL} global trend is about the same in all detectors (here in Blue2). Notice that on this Fig. detectors 1 and 4 are Hamamatsu strip photodiods, all others are BNL's Si detectors. So the global effect is approximately not detector dependent.

Extracted parameter x_{DL} shows clear correlation with event rate (Fig. 21 and 22), which indicates that pC polarimeter energy measurements are affected by high event rates. At the same time $t0$ doesn't show clear correlation with rates (Fig. 23 and 24). So using parameters x_{DL} and $t0$ we decoupled the reconstructed C-mass dependence vs fill on Fig. 9 and 10 on rate dependence of energy measurements and fill dependence of Time of Flight measurements. These rate dependencies will be discused in more details in the next section.

In the Section A.1 it will be confirmed that high rates lead to distortion of energy (as well as event rate) measurements by pC polarimeters towards lower values, leaving time of flight measurements almost unaffected. Our energy corrections from "Dead Layer" approach partially takes care about the shift in energy measurements due to rate effect. But only partially - because the energy dependence of "Dead layer" correction is not the same as from rate effect.

Unfortunately with the avilable data (including the rate effect studies during APEX sessions) we could not build a consistent quantitative picture of the dependence of the measured polarization on measured rates. One of the possible reasons for that could be that the measured rates of carbon events may not directly correlate with the total event rate in the system, which inludes prompt event rate and other backgrounds.

So eventually, the measured polarizations were corrected only for effective x_{DL} and $t0$ (like we did in all previos Runs), and systematic uncertainties were derived from the residual inconsistency in the polarization measurements by Polarimeter-1 and Polarimeter-2 and from comparison with HJet polarimeter measurements - this will be discussed below in this note.
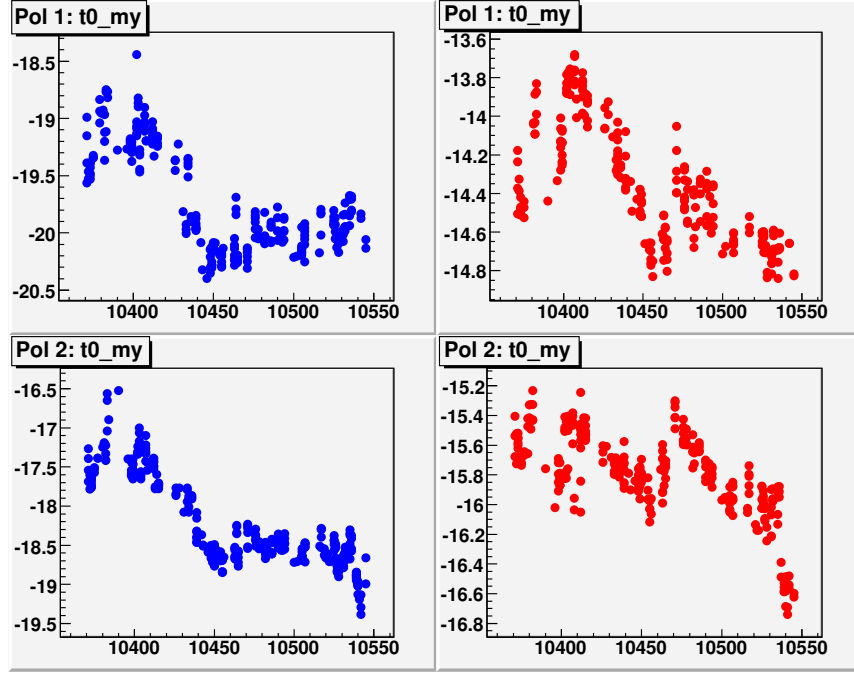
Figure 15. The average over the polarimeter strips $t0$ (ns) in $\sqrt{s}$=500 GeV measurements vs fill number (each fill usually had several measurements, all of them are shown here); top left - Blue1, bottom left - Blue2, top right - Yellow1 and bottom right - Yellow2.
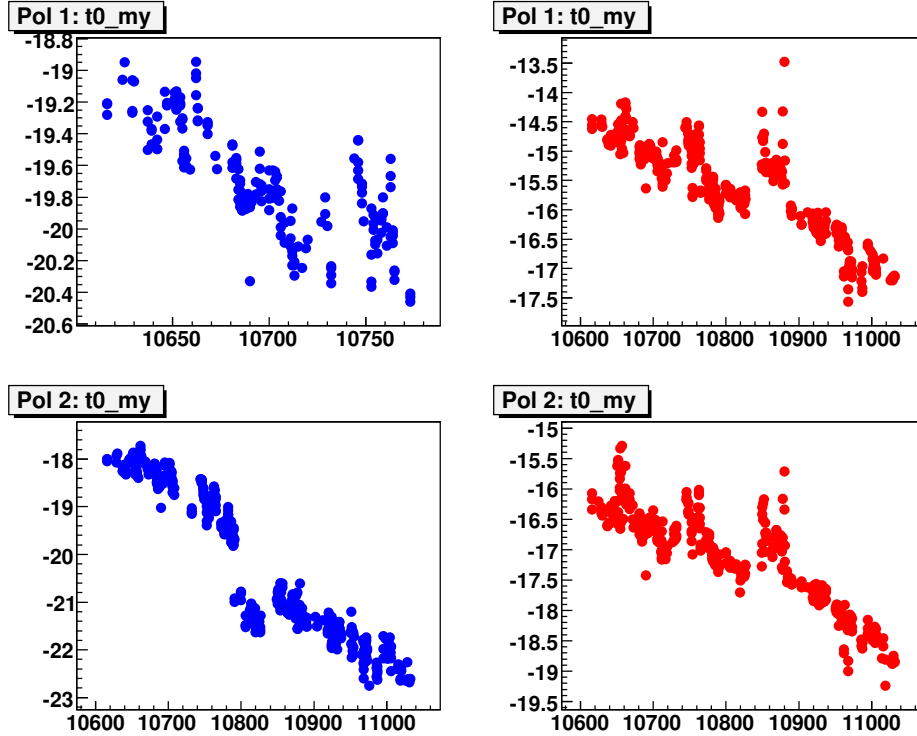

Figure 16. The same as Fig. 15, but for $\sqrt{s}$=200 GeV measurements; notice that Blue1 didn't have measurements in fills >10773.
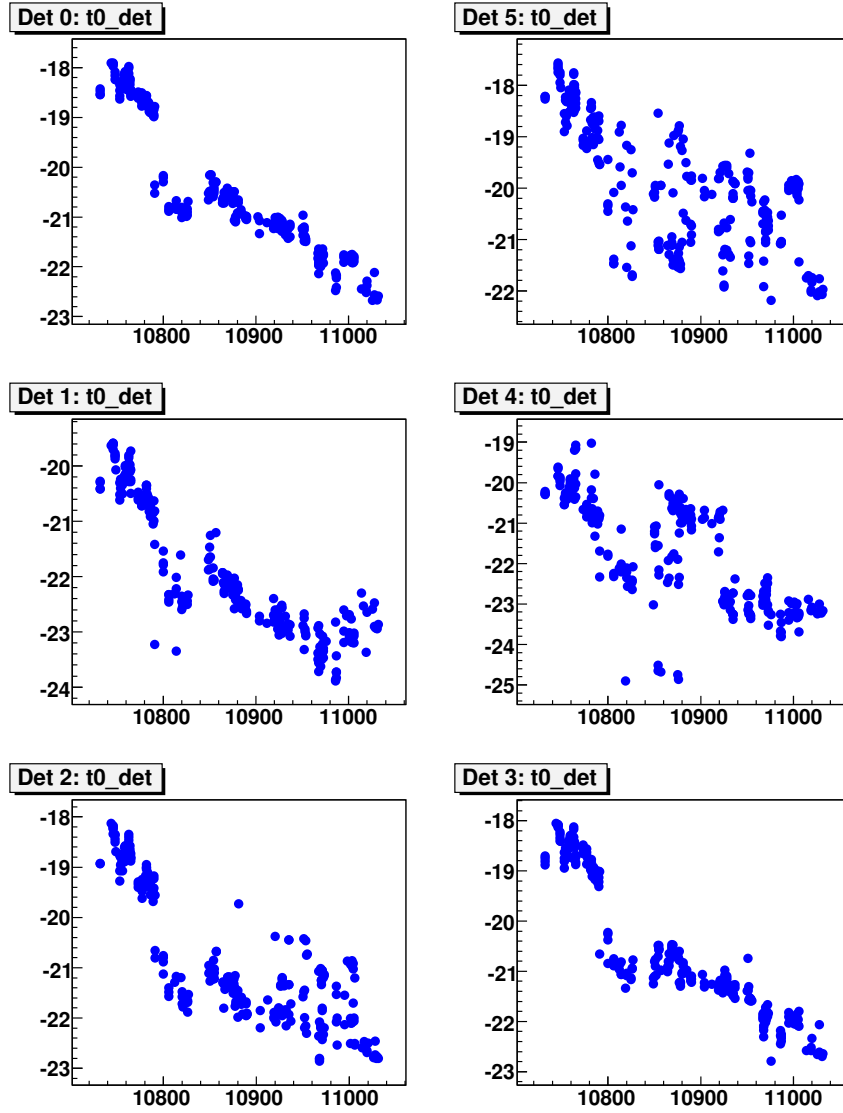
Figure 17. The average over the detector strips $t0$ (ns) in $\sqrt{s}$=200 GeV measurements by Blue2 vs fill number (each fill usually had several measurements, all of them are shown here); all 6 detectors are shown, detectors 1 and 4 (middle plots) being Hamamatsu strip photodiods, all others being BNL's Si detectors; only measurements with vertical target are shown.
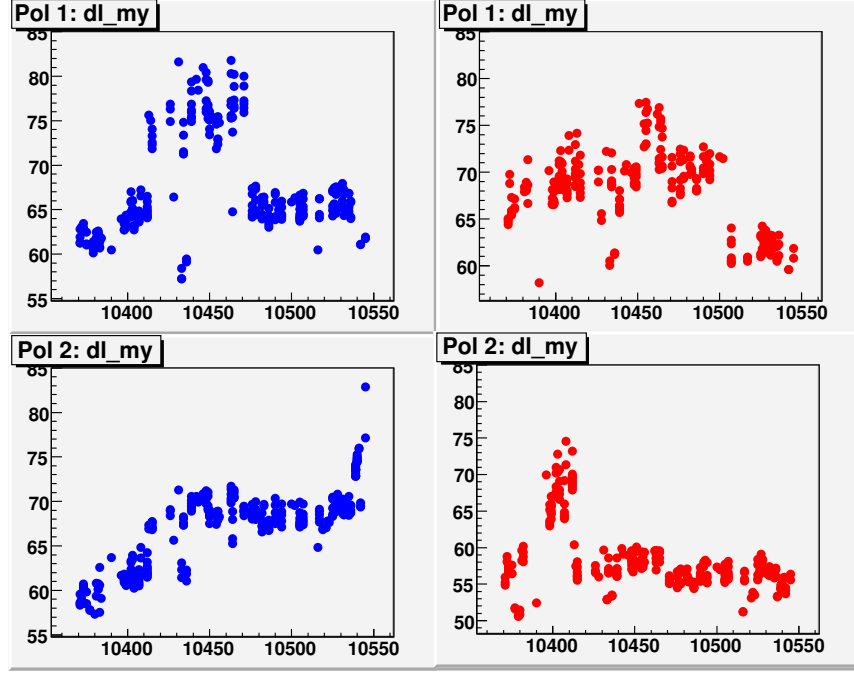
Figure 18. The average over the polarimeter strips x_{DL} (μg/cm^2) in $\sqrt{s}$=500 GeV measurements vs fill number (each fill usually had several measurements, all of them are shown here); top left - Blue1, bottom left - Blue2, top right - Yellow1 and bottom right - Yellow2.
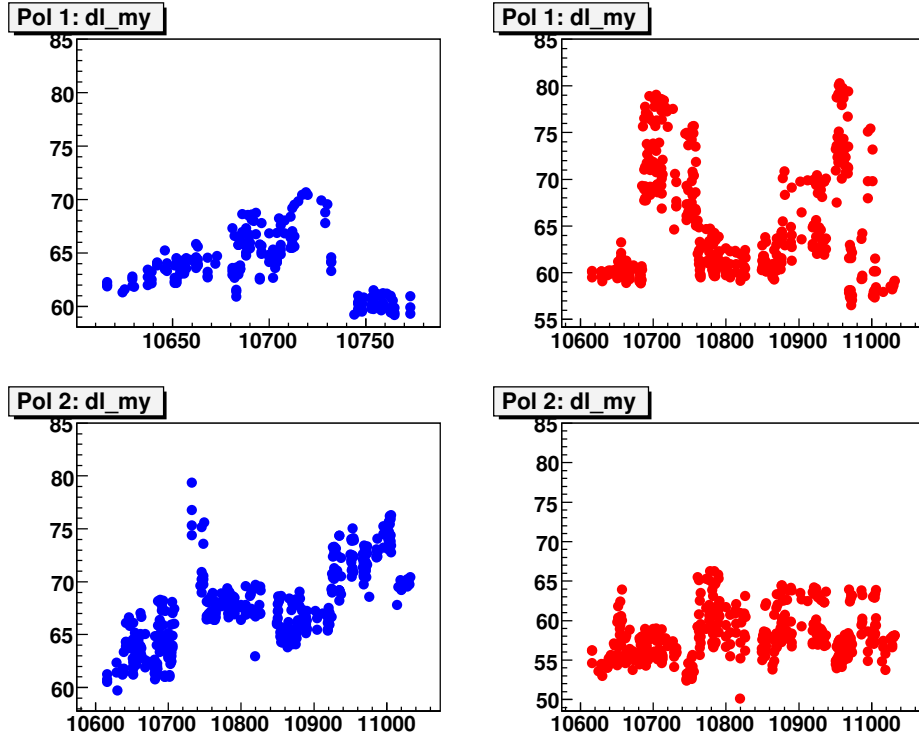

Figure 19. The same as Fig. 18, but for $\sqrt{s}$=200 GeV measurements; notice that Blue1 didn't have measurements in fills >10773.
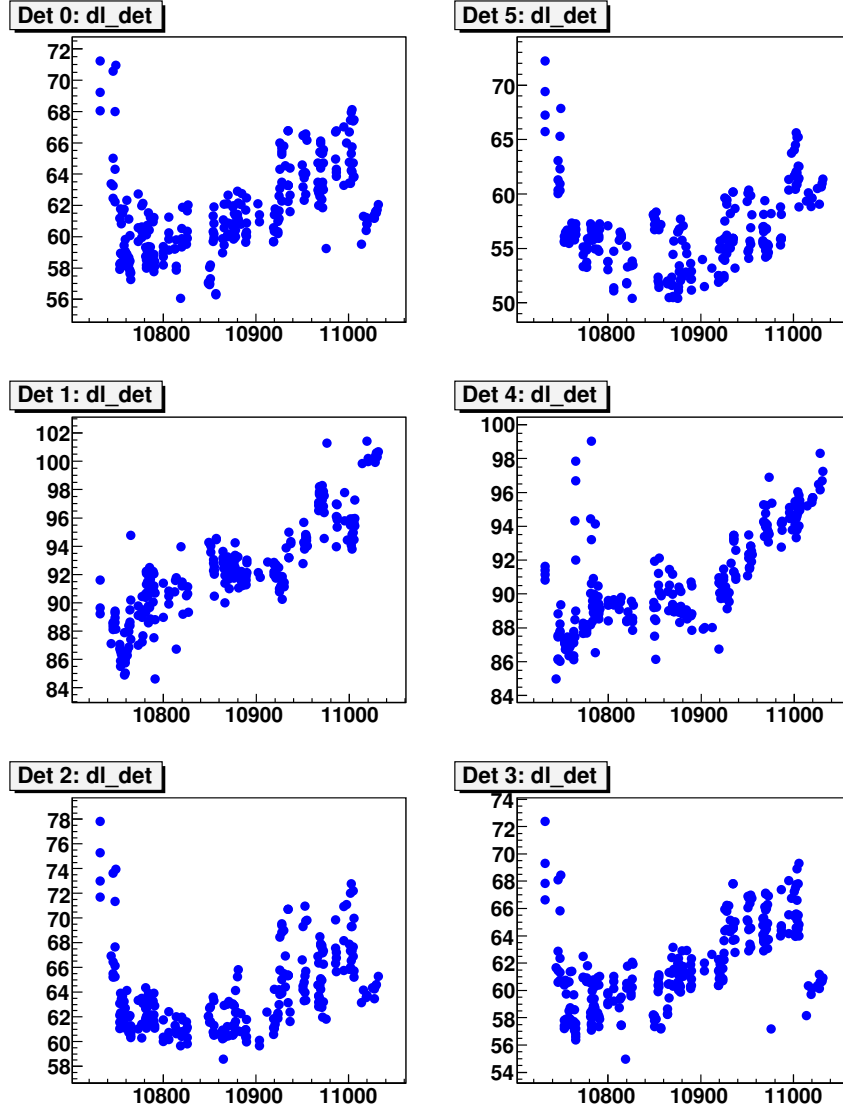
Figure 20. The average over the detector strips x_{DL} (ns) in $\sqrt{s}$=200 GeV measurements by Blue2 vs fill number (each fill usually had several measurements, all of them are shown here); all 6 detectors are shown, detectors 1 and 4 (middle plots) being Hamamatsu strip photodiods, all others being BNL's Si detectors; only measurements with vertical target are shown.
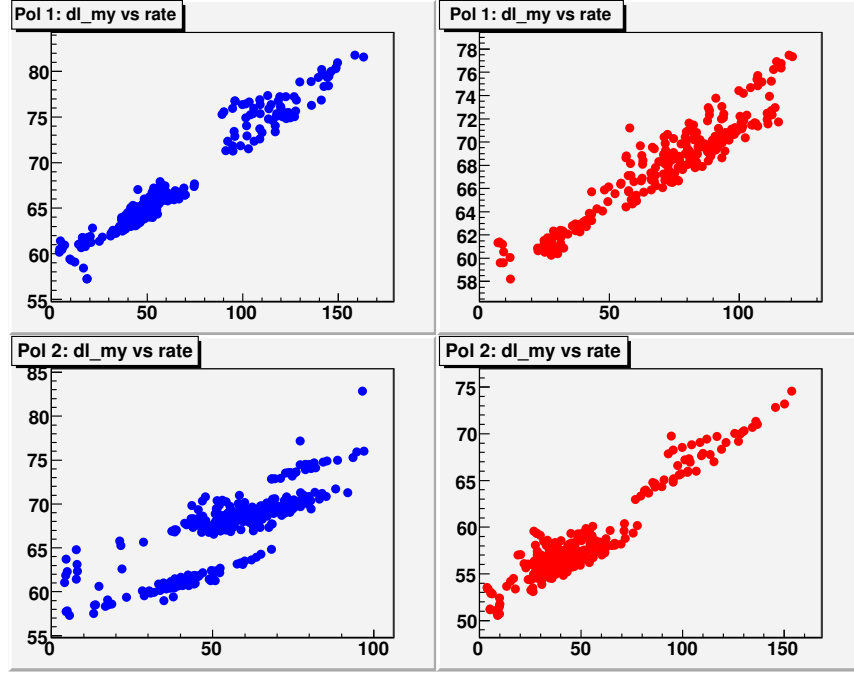
Figure 21. The average over the polarimeter strips x_{DL} (μg/cm^2) vs carbon event rate per strip (kHz) in $\sqrt{s}$=500 GeV measurements vs fill number (each fill usually had several measurements, all of them are shown here); top left - Blue1, bottom left - Blue2, top right - Yellow1 and bottom right - Yellow2.

Figure 22. The same as Fig. 21, but for $\sqrt{s}$=200 GeV measurements; notice that Blue1 didn't have measurements in fills >10773.

Figure 23. The average over the polarimeter strips $t0$ (ns) vs carbon event rate per strip (kHz) in $\sqrt{s}$=500 GeV measurements vs fill number (each fill usually had several measurements, all of them are shown here); top left - Blue1, bottom left - Blue2, top right - Yellow1 and bottom right - Yellow2.
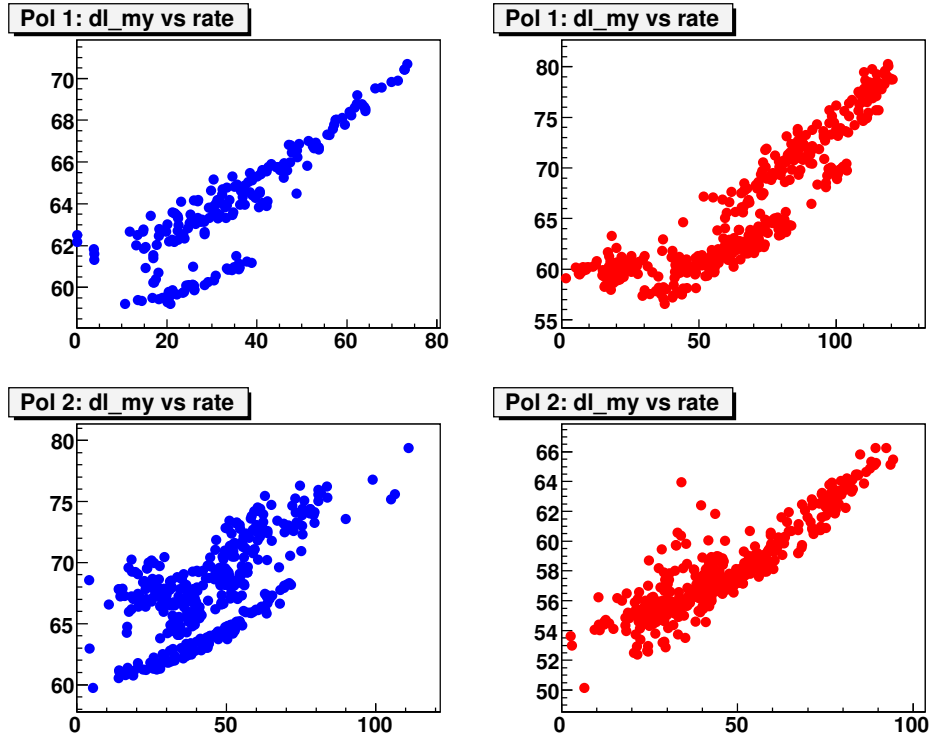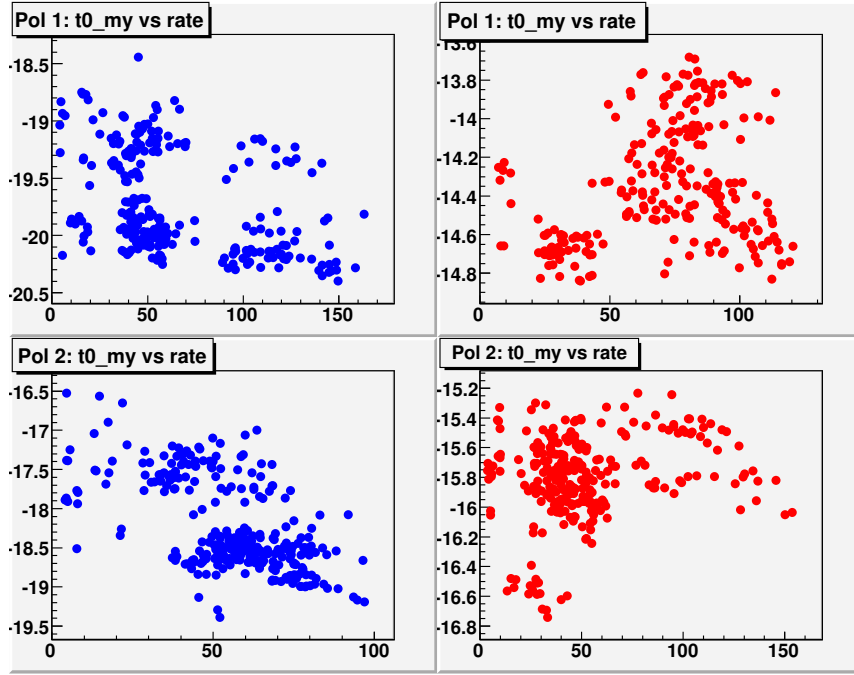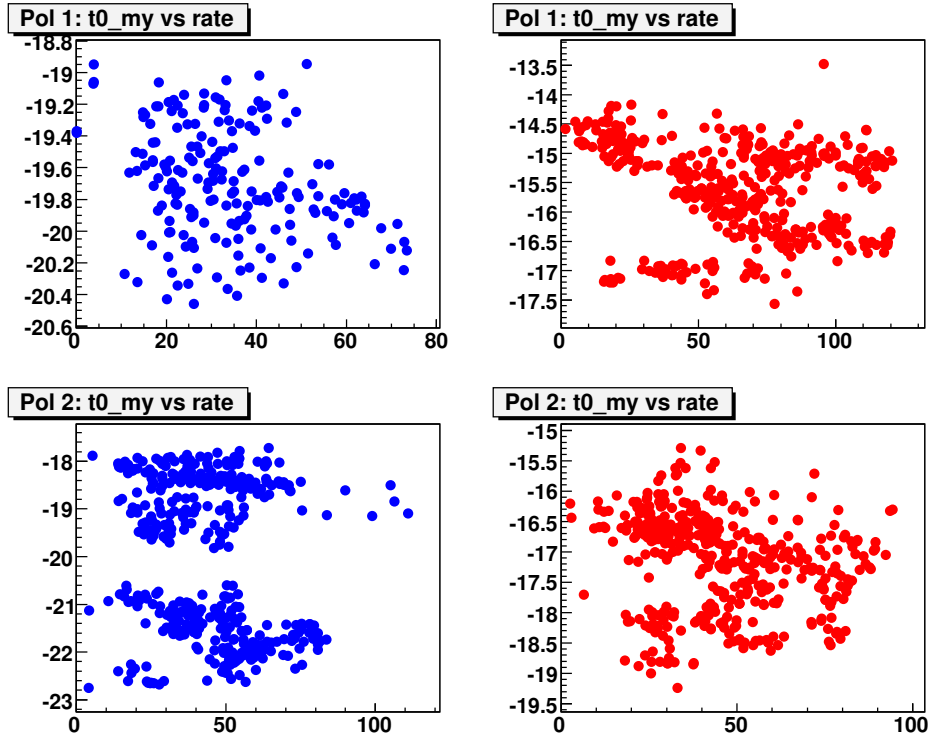

Figure 24. The same as Fig. 23, but for $\sqrt{s}$=200 GeV measurements; notice that Blue1 didn't have measurements in fills >10773.

5. Data Quality Assurance

5.1. Strip Quality Assurance

The data quality assurance was very similar to what we used in previous year analyses. The goal of Quality Assurance procedure is to identify really abnormal strips and runs. We checked strip-by-strip:

- Number of events in the banana

- Reconstructed from the fit effective dead layer x_{DL} and $t0$

- Reconstructed C-mass and width

- Non-constant behavior of reconstructed C-mass vs recoile carbon E_{kin} (in terms of RMS)

- The slope of recoile carbon energy distribution, dN/dE_{kin} vs E_{kin} (in terms of the slope of the fit to exp)

From the final polarization analysis we excluded Hamamatsu detectors in Blue2 and Yellow2 polarimeters (Hamamatsu detectors from Yellow2 were not in the common data stream anyway). We did so not only to be able to perform more uniform analysis (with only one type of detectors), but also due to too large variations in the slope of dN/dE_{kin} vs E_{kin} in Hamamatsu detectors in Blue2 as it is shown on Fig. 52 and 53.

The test of the "Number of events in the banana" helped us to discover a few very noisy channels in Blue2 of detector 1 (Hamamatsu strip) - strips 15, 17 and 19 - which affected also strips (33, 35, 37), (51, 53, 55) and (69, 71, 1) which are connected to the same WFD. All these strips were excluded from the analysis. Channel 33 in Blue1 also from time to time demonstared instabilities and was excluded from many measurement analysis. These problems in channel 33 were also noticed in alpha calibration runs (see Section 2).

Channels 53 and 55 were very noisy in Yell1, so they were disconnected and were not used in the data analysis (and data collection). Channel 70 often in Yell1 and occatioanally in Yell2 showed very few (or no) events in banana cut, so was excluded from these measurements. Strip 34 in both Yell1 and Yell2 showed too sharp slope for Ekin distribution (about twice sharper than other strips), so was excluded from the final analysis.

Time of flight measurements in several WFDs in yellow fills 10850 and 10851 showed a jump by ~ 8 ns (and after that back to normal). Besides that data didn't show any other abnomalities, so that after correction for this time offset data was used in the final anaysis.

Table 1 showes a summary of major problems discovered during strip QA procedure. In addition to the masked strips mentioned in the table some measurements had 1-2 more strips masked due to different reasons (listed in the beginning of this section).

5.2. Bunch Quality Assurance

As in previous years we didn't use bunch 20 in our analysis, because it was used for RHIC fill setup and tune, so it usually showed different behavior (emittance etc.) compared to other bunches. Bunch 0 was also masked in our analysis because it was used to

Table 1
QA summary

Strip(s)	Problem	Pol@$\sqrt{s}$	Masked
33	Instabilities in amp	Blue1@200GeV	occasionally
Det 1 and 4	E_{kin} slope	Blue2@200GeV	all measurements
33,35,37,51,53,55,69,71,1	Because of noisy strips 15,17,19	Blue2@200GeV	all measurements
53,55	Too noisy	Yell1@200GeV	all measurements
70	Too few C events	Yell1@200GeV	occasionally
34	E_{kin} slope	Yell1@200GeV	all measurements
70	Too few C events	Yell2@200GeV	occasionally
34	E_{kin} slope	Yell2@200GeV	all measurements
33	Instabilities in amp	Blue1@500GeV	occasionally
Det 1 and 4	E_{kin} slope	Blue2@500GeV	all measurements
33,35,37,51,53,55,69,71,1	Because of noisy strips 15,17,19	Blue2@500GeV	all measurements
53,55	Too noisy	Yell1@500GeV	all measurements
70	Too few C events	Yell1@500GeV	occasionally
34	E_{kin} slope	Yell1@500GeV	all measurements
70	Too few C events	Yell2@500GeV	occasionally
34	E_{kin} slope	Yell2@500GeV	all measurements

inject generator pulses in the system for monitoring purposes. Due to instabilities of the amplitude and time position of the pulses they sometimes overlapped with C events in the banana.

Unlike previous year analyses, in this analysis we didn't reject measurements based on our usual control of the consistency of bunch-by-bunch asymmetry and "specific" luminosity (bunch event rate normalized by bunch intensity). This inconsistency (in the first bunches compared to other bunches) used to show up in the past when very thick target was accidently put in the beam. In 2009, particularly in $\sqrt{s} = 500$ GeV data we very often had such an inconsistency due to high event rates in the polarization measurements (on the average $\sim 2 - 4$ times higher than in previous years). An example of such a measurement is shown on Fig. 48 and 49. As will be discussed in Section A.1, this inconsistency may come from bunch dependence of rate effect and slightly different response of detectors to high rates, which lead to bunch dependent detector asymmetry. Since the average over bunches detector asymmetry in our analysis is properly taken out from the physics asymmetries, this inconsistency in the asymmetry measurements among bunches should not directly affect the polarization results. This was confirmed in a few measurements when we compared polarizations measured in the first 20 bunches (where the effect is maximal) vs last 20 bunches (where there is no effect) and found consistency within statistical errors.

6. Polarization measurements

6.1. Polarimeters-1 vs Polarimters-2

Fig. 25 and 26 show the comparison of polarization measurements by Polarimeter-1 and Polarimeter-2 in blue and yellow rings. As it is particularly obvious from $\sqrt{s}$=500 GeV, the variation of the ratio of the measurements by two polarimeters is not statistical. If points on bottom plots are projected on vertical axis the Mean/RMS are 0.96/0.09 and 0.92/0.11 for blue and yellow for $\sqrt{s}$=500 GeV and 0.972/0.049 and 1.000/0.059 for blue and yellow for $\sqrt{s}$=200 GeV. These inconsistencies, $\sim$12% for $\sqrt{s}$=500 GeV and $\sim$6% for $\sqrt{s}$=200 GeV will be included in the fill-by-fill systematic uncertainties in our measurements. Online polarization values gave slightly larger discrepancies between measurements in two polarimeters: 0.90/0.09 and 0.87/0.12 for blue and yellow for $\sqrt{s}$=500 GeV 0.917/0.052 and 0.953/0.074 for blue and yellow for $\sqrt{s}$=200 GeV. It means that applied energy corrections partially removed the systematics in our measurements.

6.2. Polarization profile

Polarization profile is one of the key issues in proton beam polarization measurements at RHIC. Scanning carbon ribbon target across the beam allows to measure beam intensity and polarization profiles in both vertical and horizontal directions in transverse plane. For non-flat polarization profile the beam polarization will be seen differently by H-Jet polarimeter, pC polarimeter (in fixed target measurement mode) and when colliding beams in the interaction regions of RHIC experiments. Due to that the jet target in H-Jet polarimeter is much wider than beam width, the polarization profile is weighted with beam intensity profile in the average beam polarization. For colliding beams, the polarization profile is weighted with a product of two beam intensity profiles in transverse plane. The polarization measurement in pC polarimeter will depend on the positioning of the carbon target, and on whether horizontal or vertical target is used for the measurements (in case beam horizontal and vertical profiles are different).

Assuming gaussian profiles ($I(x, y)$ for intensity and $P(x, y)$ for polarization), the average beam polarization seen by H-Jet polarimeter can be expressed:

$$\langle P \rangle_{HJet} = \frac{\iint P(x, y)I(x, y)dxdy}{\iint I(x, y)dxdy} = \frac{P_{max2}}{\sqrt{(1 + R_X) \cdot (1 + R_Y)}}, \tag{2}$$

by pC polarimeter for the case with vertical target positioned at beam maximum intensity (and polarization) along X axis:

$$\langle P \rangle_{pC-maxX} = \frac{\int P(y)I(y)dy}{\int I(y)dy} = \frac{P_{max2}}{\sqrt{(1 + R_Y)}}, \tag{3}$$

and similarly for $\langle P \rangle_{pC-maxY}$ using horizontal target; and by experiments in two beam collision, for $I_{1,2}$ relating to intensity profiles for two beams respectively:

$$\langle P \rangle_{Exp} = \frac{\iint P(x, y)I_1(x, y)I_2(x, y)dxdy}{\iint I_1(x, y)I_2(x, y)dxdy} = \frac{P_{max2}}{\sqrt{(1 + \frac{1}{2}R_X) \cdot (1 + \frac{1}{2}R_Y)}}, \tag{4}$$

with P_{max2} the polarization at beam maximum intensity and polarization in transverse plane (in 2-dim), R_X and R_Y the squared ratio of the intensity profile width and polarization profile width $(\sigma_I/\sigma_P)^2$, for X and Y projections respectively.
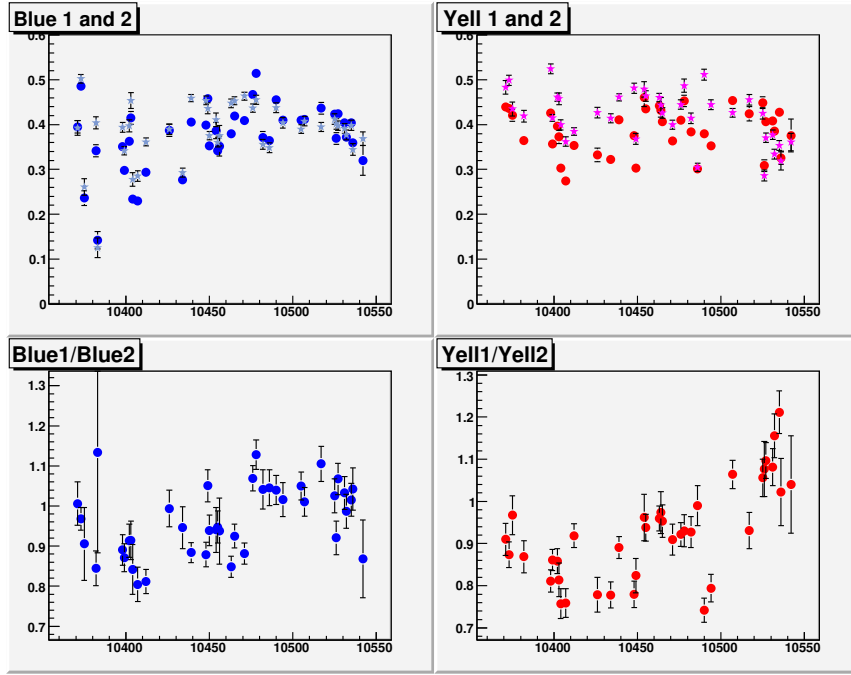
Figure 25. Fill-by-fill polarizations (weighted average over measurements in a fill) in $\sqrt{s}$=500 GeV part of Run9 (neither yet normalized to HJet nor corrected for pol. profile), by Blue1 (blue circles) and Blue2 (light blue starts) on top left, by Yell1 (red circles) and Yell2 (pink starts) on top right; fill-by-fill comparison of polarization measurements: Blue1/Blue2 on bottom left, and Yell1/Yell2 on bottom right.
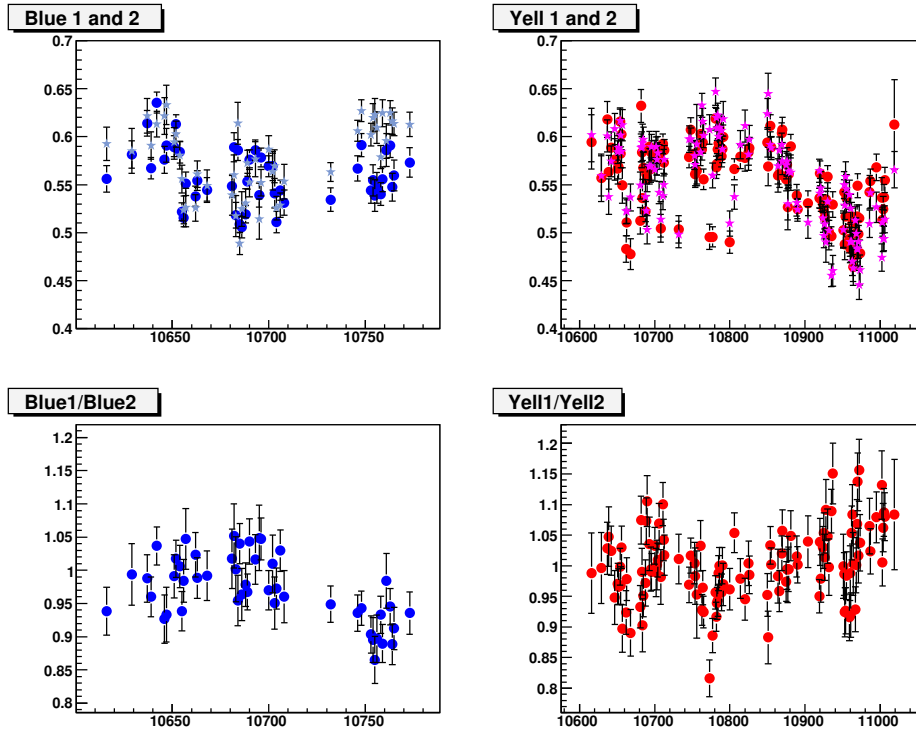

Figure 26. The same as Fig. 25, but for $\sqrt{s}$=200 GeV measurements; notice that Blue1 didn't have measurements in fills >10773.

These relations between average polarizations are taken into account when normalizing pC measurements to H-Jet absolute polarization measurements and when providing polarization values for RHIC experiments.

The profile parameters R_X and R_Y can be extracted from the direct measurements of σ_I and σ_P in case the measured profiles are not corrupted. Currently we see two effects which corrupt the measured profiles. One is rate effect, which was clearly seen in Run9 when event rates were high (see for example Fig. 28). Another one was observed in pretty low rate conditions starting from Run6 (when we first started measuring profiles in each physics fill), an example from Run9 is shown on Fig. 29. From our current view, this effect is seen in cases we use loose (usually thin) target which is attracted to the beam center when it is moved into the beam, so that effectively target is stuck in the beam center instead of moving across the beam with uniform speed. In the this case to extract profile parameter R we can use a correlation between polarization and intensity in each target position:

$$\frac{P}{P_{max}} = \left(\frac{I}{I_{max}}\right)^R \tag{5}$$

which doesn't require knoweledge on target position. I_{max} and P_{max} are beam intensity and polarization, respectively, when target is positioned in the beam center. Notice, I_{max} and P_{max} here are in 1-dim space (either in X or Y), because they are averaged in the other transverse direction - along target orientation; P_{max} and R here carry the meaning of $\langle P \rangle_{pC-maxX}$ and R_X or $\langle P \rangle_{pC-maxY}$ and R_Y depending on target orientation. From the fit to data we extract parameters P_{max} and R, from which we can get the average polarization across the beam (to be compare to HJet measurements, when determining the normalization for pC measurements):

$$\langle P \rangle = \frac{P_{max}}{\sqrt{1+R}}. \tag{6}$$

This is the approach used in previous years analyses. Fig. 30 and 31 show the fill by fill measurement of profile parameter R using the polarization-intensity correlation.

Currently we do not have a clear view how to correct rate effect on profile measurements, which tend to give a bias to flatter polarization profile as it is seen on Fig. 32 and at smaller extent on Fig. 33 (parameter R gets closer to 0). If we assume that polarization profile parameter R is properly reconstraucted at low rates, we can rely on the measurements of R near rate ~ 0, which was ~ 0.4 for 250 GeV beams and ~ 0.08 for 100 GeV beams, similar in both transverse projections. Very similar to 100 GeV beam measurements value of R was obtained in the measurements at RHIC injection and AGS [4].

To get even more firm statement about polarization profiles in Run9 (and to double check the conclusion about profile we have just made above), we selected only good measurements, when intensity profile was gaussian (not corrupted), as for example one shown on Fig. 27. Fig. 34 and 35 summarize such measurements in Run9 data, which confirm our conclusion about the average polarization profile parameters R of ~ 0.4 for 250 GeV beams and ~ 0.08 for 100 GeV beams in Run9. Results are summarized in Table 2.
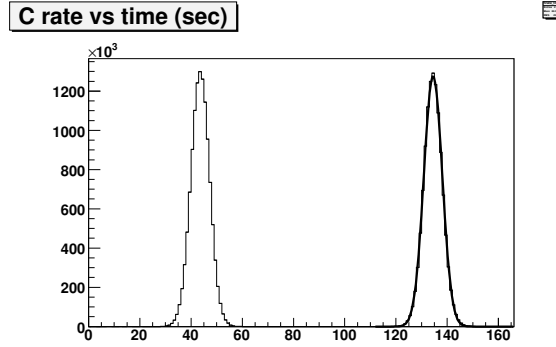
Figure 27. Measurement 10616.005 (Blue1 at $\sqrt{s} = 200$ GeV): event rate in the "banana" in 1 sec bins; fit of the second peak to gaussian is shown for the comparison; this is an example for uncorrupted profile
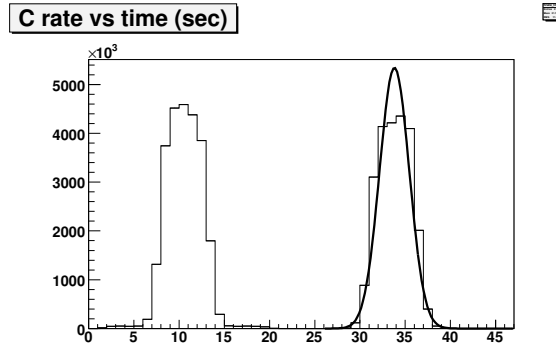

Figure 28. The same as Fig. 28, but for the measurement 10689.005 (Blue1 at $\sqrt{s} = 200$ GeV); this is an example with high rate.
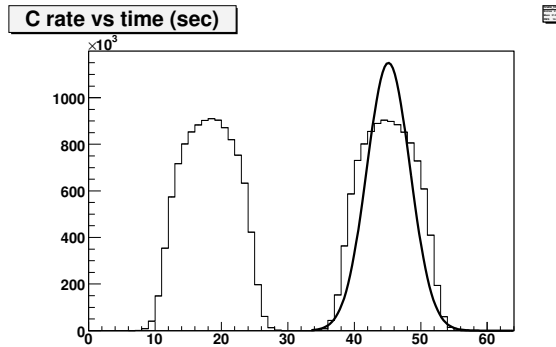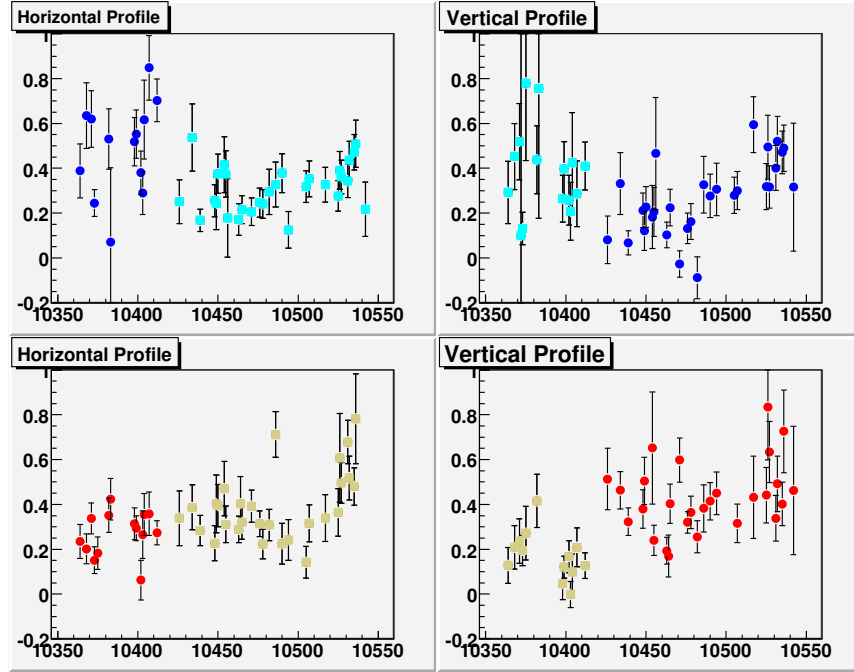

Figure 29. The same as Fig. 28, but for the measurement 10616.206 (Blue2 at $\sqrt{s} = 200$ GeV); this is an example with low rate.

Figure 30. Polarization profile parameter R vs fill in $\sqrt{s}$=500 GeV data: left plots for horizontal profile, right plots for vertical profile, upper plots for blue ring, bottom plots for yellow ring; circles for polarimeter-1, squares for polarimeter-2.
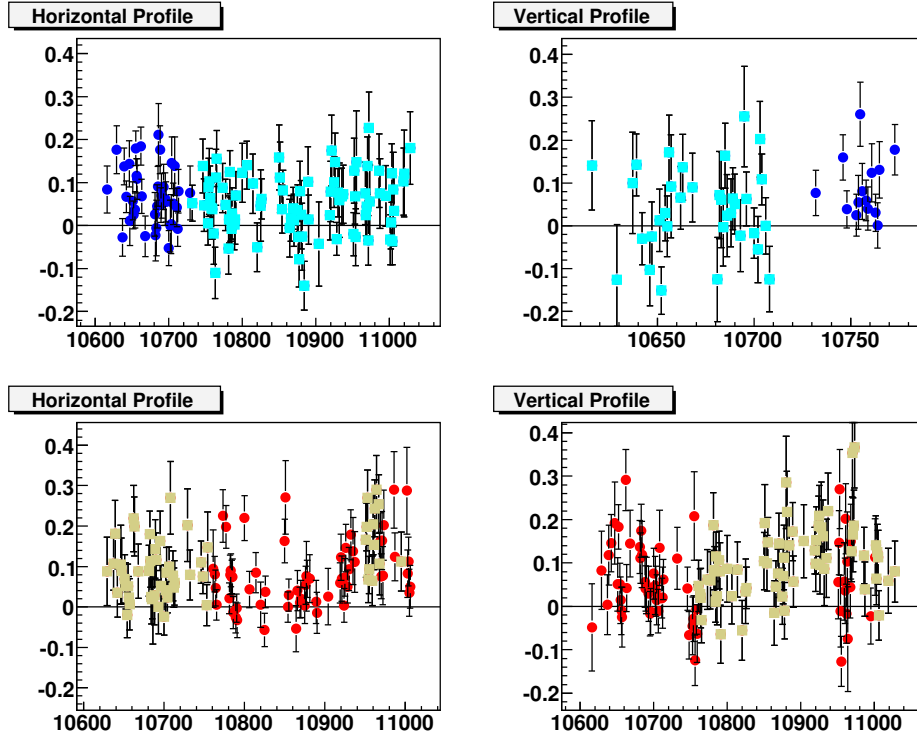
Figure 31. The same as Fig. 30, but for $\sqrt{s}$=200 GeV data.
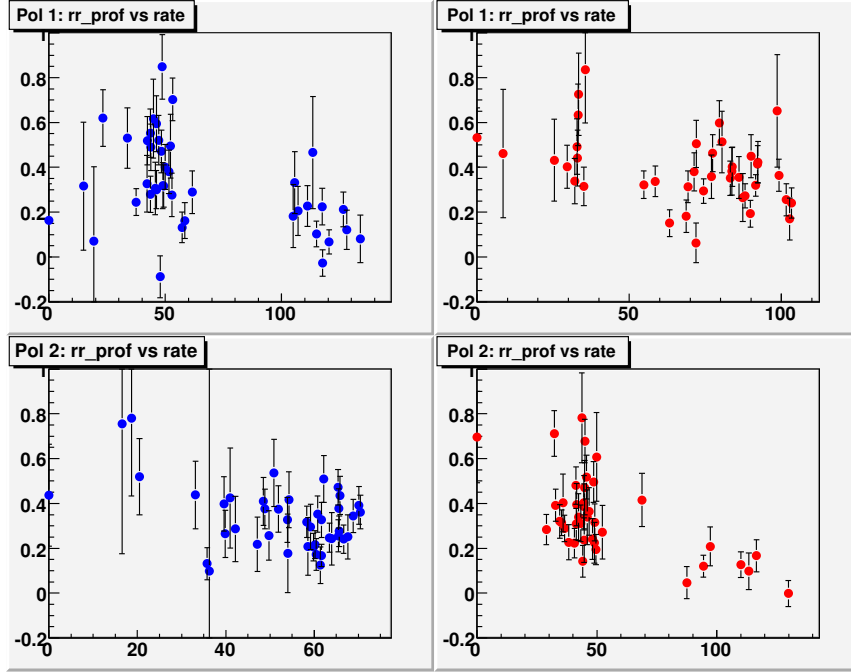
Figure 32. Polarization profile parameter R vs rate per strip (kHz) in $\sqrt{s}$=500 GeV data measured by Blue1 (upper-left), Blue2 (bottom-left), Yell1 (upper-right) and Yell2 (bottom-right). Data for horizontal and vertical profiles are shown together.
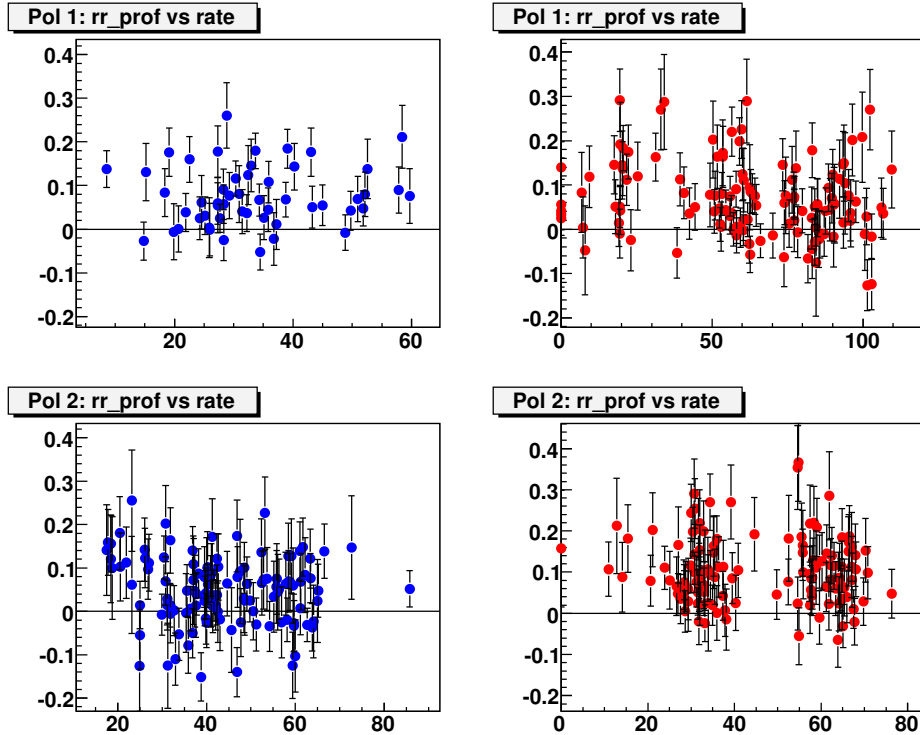
Figure 33. The same as Fig. 32, but for $\sqrt{s}$=200 GeV data.
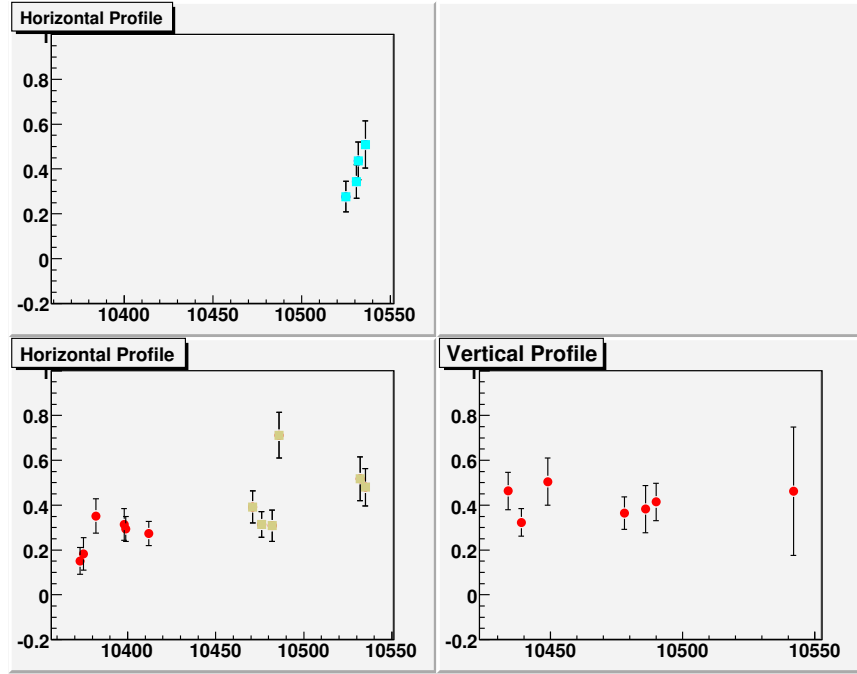
Figure 34. The same as Fig. 30, but only for data with gaussian intensity profiles (at $\sqrt{s} = 500$ GeV).
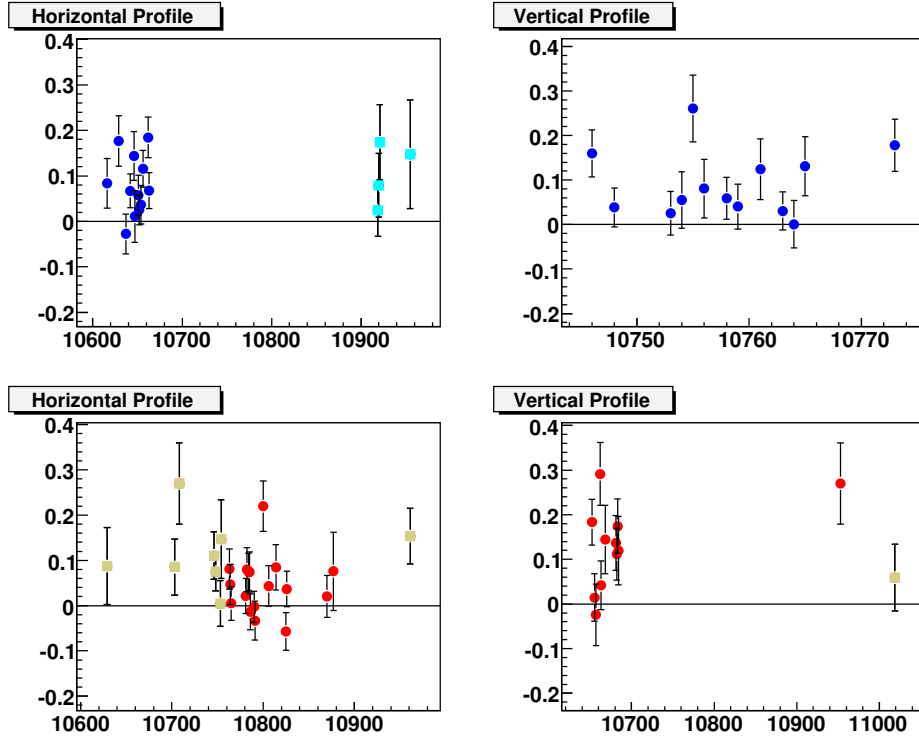

Figure 35. The same as Fig. 31, but only for data with gaussian intensity profiles (at $\sqrt{s} = 200$ GeV).

Table 2
Average over fills polarization profile parameter R. For "low rate" case we used data with rates < 30 kHz/strip (notice, only few points satisfied "low rate" condition at $\sqrt{s} = 500$ GeV (see Fig. 30), so the corresponding numbers can not represent the average R from the whole data sample).

$\sqrt{s}, GeV$	Blue-Horiz	Blue-Vert	Yell-Horiz	Yell-Vert
500, from Fig. 30 (all)	0.29 ± 0.02	0.22 ± 0.02	0.31 ± 0.02	0.27 ± 0.02
500, from Fig. 30 (low rate)	0.63 ± 0.09	0.49 ± 0.10	0.31 ± 0.07	0.41 ± 0.08
500, from Fig. 34 (good prof)	0.37 ± 0.04	—	0.32 ± 0.03	0.39 ± 0.03
200, from Fig. 31 (all)	0.053 ± 0.005	0.050 ± 0.010	0.067 ± 0.005	0.066 ± 0.006
200, from Fig. 31 (low rate)	0.061 ± 0.011	0.076 ± 0.015	0.076 ± 0.015	0.089 ± 0.014
200, from Fig. 35 (good prof)	0.073 ± 0.012	0.075 ± 0.015	0.056 ± 0.010	0.117 ± 0.018

Despite that in Run9 parameter R was supposed to be determined in both transverse directions from scan measurements in each physics fill (by polarimeter-1 in one projection and by polarimeter-2 in the other projection), there were only a few fills which provided reliable measurement of R. We decided to use the same R parameter for all fills (from the average in "good prof" measurements in Table 2), 0.36 for for $\sqrt{s} = 500$ GeV and 0.08 for for $\sqrt{s} = 200$ GeV measurements, with fill-by-fill uncertainty ± 0.36 and ± 0.08, respectively, which roughly reflects the range of variation of R from fill to fill as from Fig. 30, 31, 34 and 35. The uncertainty on the average of R should enter the global polarization uncertainty (correlated for all fills, separately for $\sqrt{s} = 500$ GeV and 200 GeV measurements). From the (maximal) variation of numbers in Table 2 relative to average values of 0.36 and 0.08, it was (over)estimated to be ± 0.14 and ± 0.04, for $\sqrt{s} = 500$ GeV and 200 GeV, respectively.

6.3. Normalization to HJet

Normaliztion for pC measurements is obtained from the comparison of HJet measurements with the average beam polarization $\langle P \rangle$ across beam transverse profile obtained by pC. The latter can be taken from a scan measurement P_{scan}, which biases the true value of $\langle P \rangle$ in case we have rate or "loose target" problems. For "loose target" measurements the unbiased value of $\langle P \rangle$ can be obtained using Eq. (6). At the same time this approach makes the estimation even worse (compared to just $\langle P \rangle_{pC}$ from the scan) for the measurements suffering from high rates. Since in our data we can not clearly separate these two effects, we decided to use P_{scan} for the evaluation of $\langle P \rangle$ by pC.

Fig. 36, 37, 38, 39 show the comparison of HJet over pC measurements as well as their ratio, fill by fill for all four pC polarimeters. All data are consistent with a constant behavior vs fills (within large stat. uncertainites coming mainly from HJet uncertainties).

To make a more precise test, on Fig. 40, 41, 42 and 43 we compares HJet and pC measurements vs periods (luminosity weighted average over fills in a group), defined by the group of fills where the target in polarimeter-1 and polarimeter-2 didn't change (separately for blue and yellow). On this level we also do not see any obvious signs of systematic problems in the comparison of HJet and pC measurements.
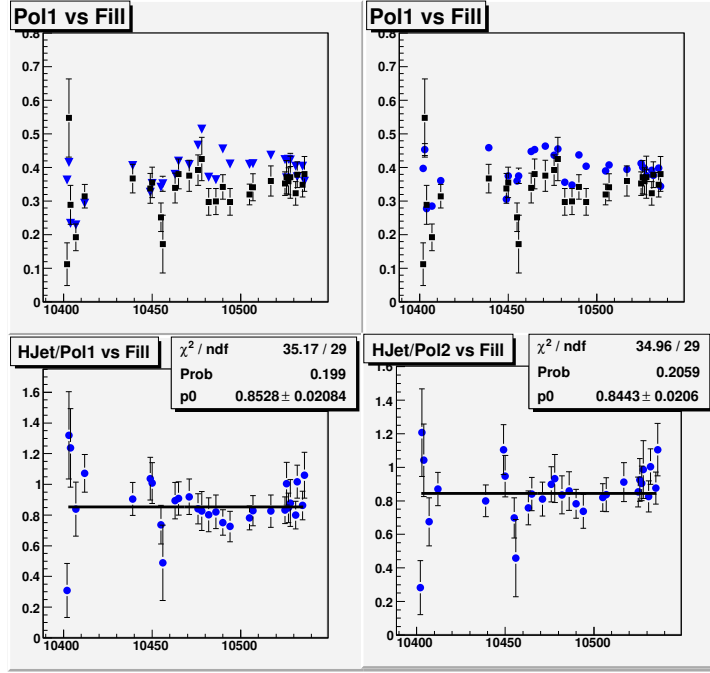
Figure 36. Upper plots: comparison of fill-by-fill polarizations measured by HJet (black squares) and pC in blue ring at $\sqrt{s}$=500 GeV, left for Blue1, right for Blue2; Bottom plots: ratio of HJet over pC polarizations, fill by fill, left for Blue1, right for Blue2.
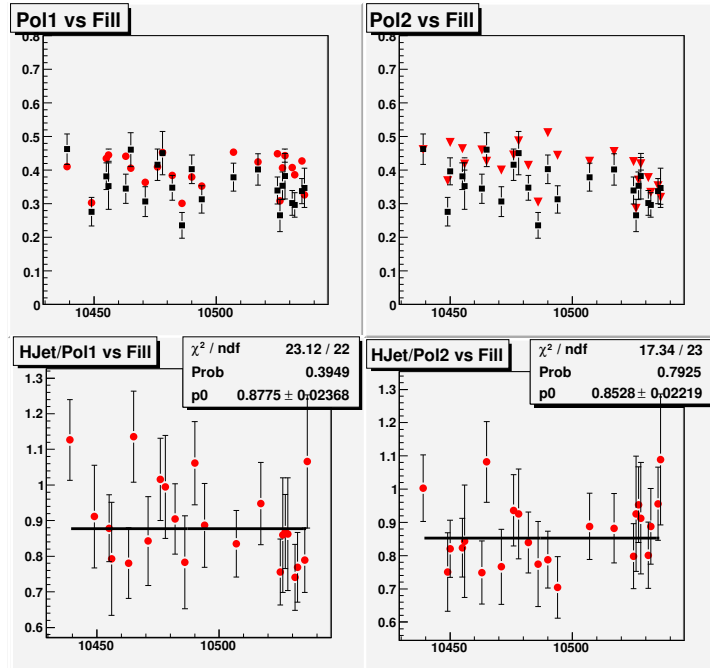

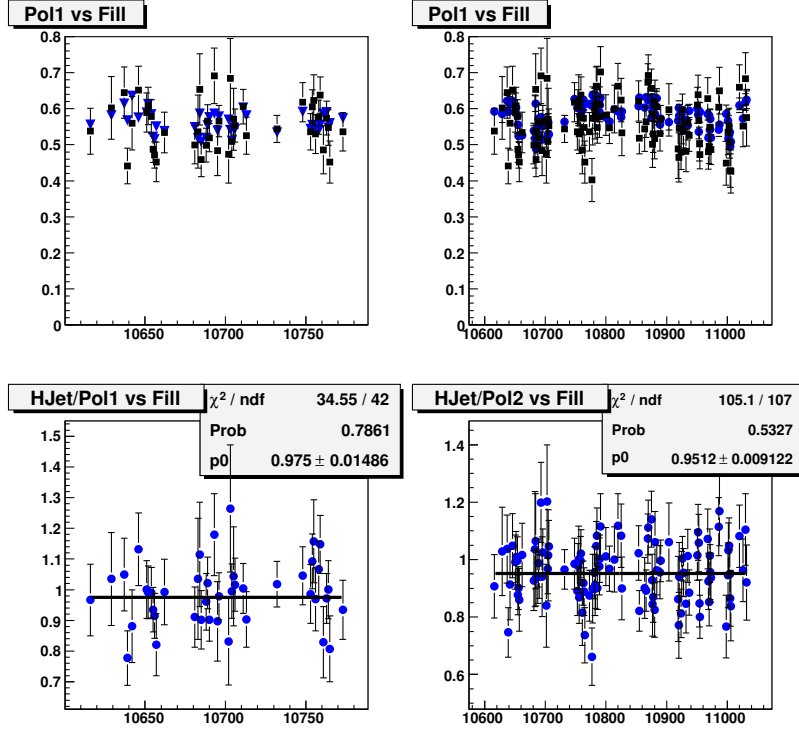Figure 37. The same as Fig. 36, but for yellow ring at $\sqrt{s}$=500 GeV.

Figure 38. The same as Fig. 36, but for blue ring at $\sqrt{s}$=200 GeV.
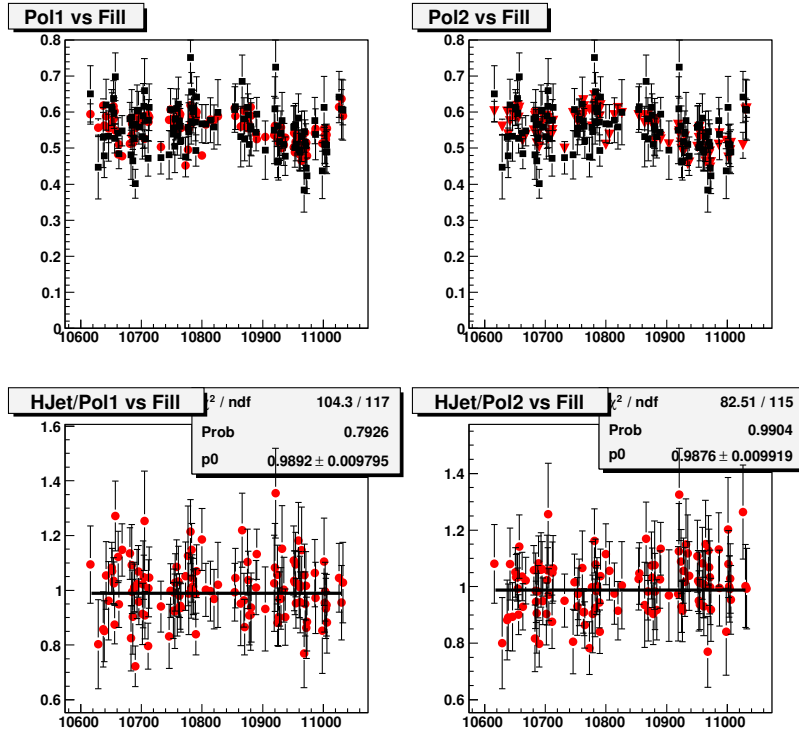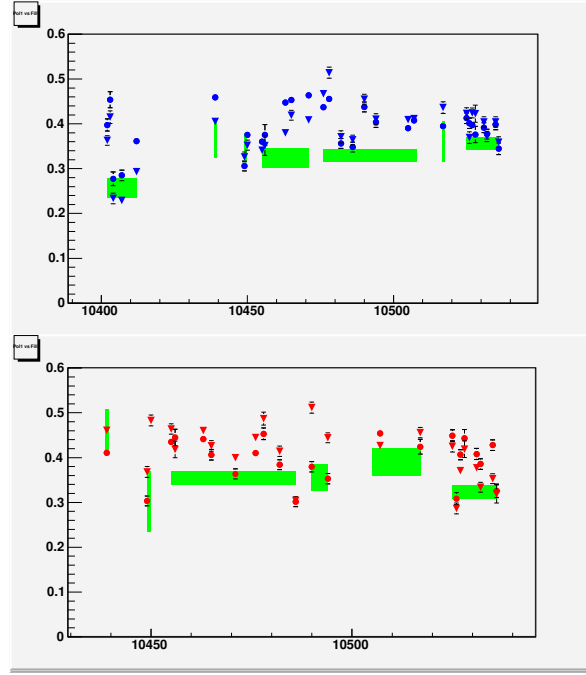

Figure 39. The same as Fig. 36, but for yellow ring at $\sqrt{s}$=200 GeV.

Figure 40. Comparison of fill-by-fill pC polarization measurements (triangles for polarimeter-1 and circles for polarimeter-2) with HJet measurements averaged over groups of fills denoted by horizontal spread of the green rectangles, vertical size of the rectangles being $\pm 1\sigma$ stat. error for a period; data for $\sqrt{s} = 500$ GeV blue (upper) and yellow (bottom). pC measurements are shown only for fills which also have HJet values.
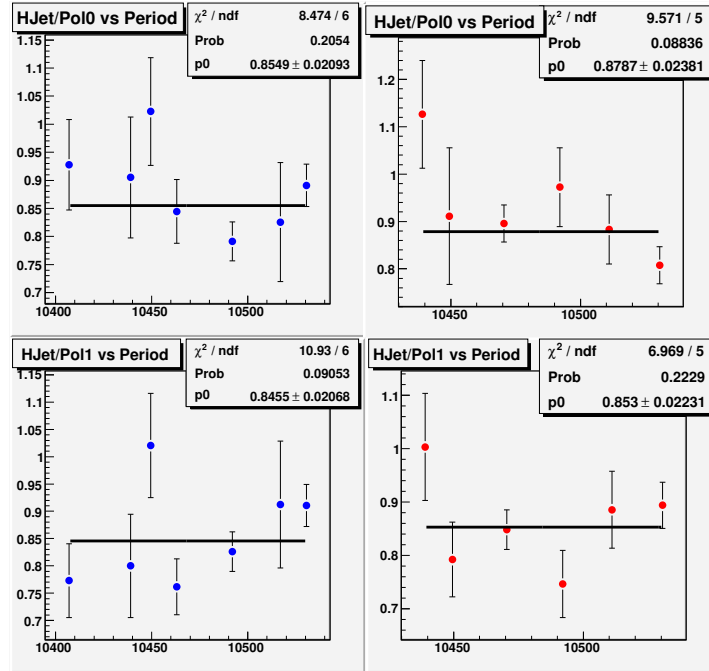
Figure 41. Ratio of the HJet polarization measurements over pC measurements, period-by-period; periods are defined by a group of fills where the target in polarimeter-1 and polarimeter-2 didn't change (separately for blue and yellow); upper left for Blue1, bottom left for Blue2, upper right for Yell1, bottom right for Yell2.
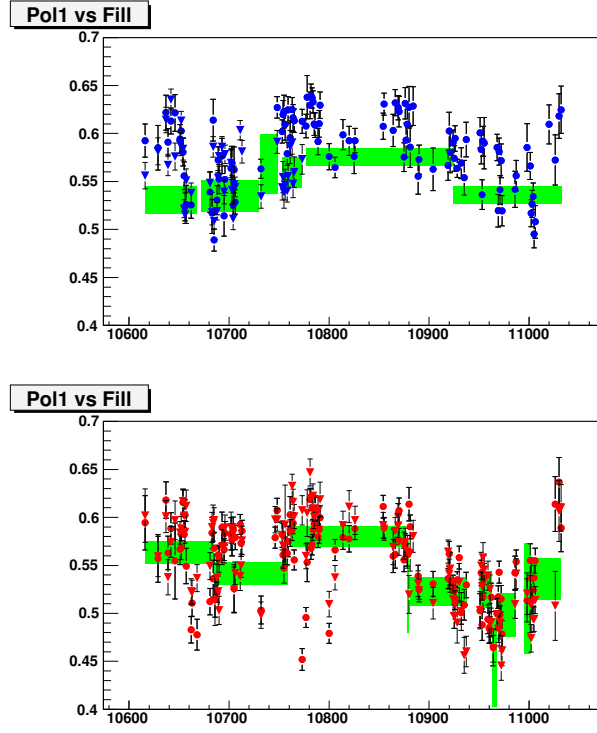
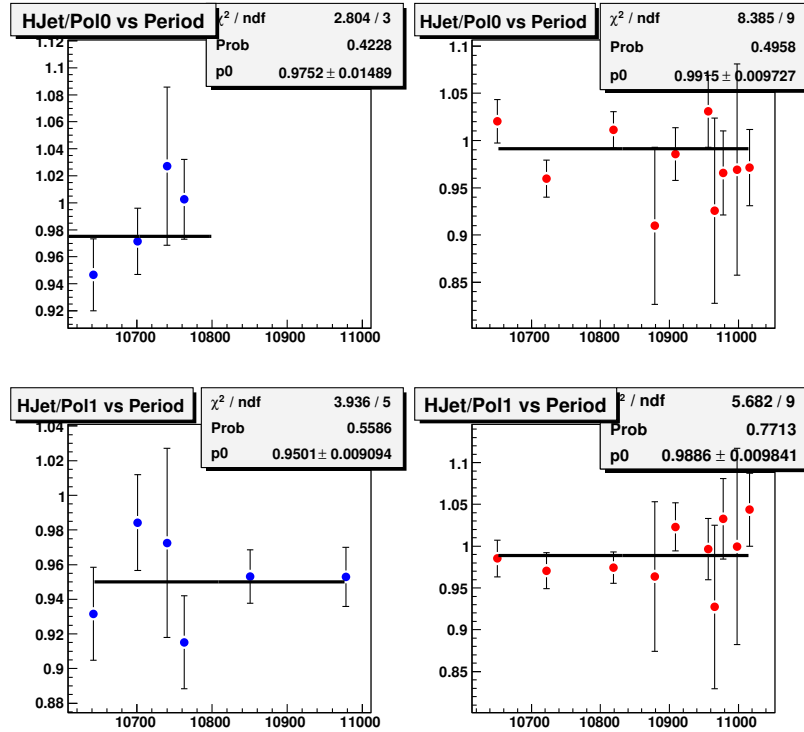Figure 42. The same as Fig. 40, but for $\sqrt{s}$=200 GeV.

Figure 43. The same as Fig. 41, but for $\sqrt{s}$=200 GeV.

The normalization for the pC measurements was obtained from the comparison of HJet measurements and pC measurements averaged over the whole run, separetely for each pC polarimeter and for $\sqrt{s} = 200$ and 500 GeV. HJet average polarization over the run is obtained from fill combined statistics (which effectively is luminosity weighted); pC average polarization was obtained from fill polarizations weighted with the number of HJet events in a fill. Results are shown in Table 3.

Table 3
Normalization factor for pC measurements; errors are stat. only.

$\sqrt{s}, GeV$	Blue1	Blue2	Yell1	Yell2
500	0.000 ± 0.000	0.000 ± 0.000	0.000 ± 0.000	0.000 ± 0.000
200	0.000 ± 0.000	0.000 ± 0.000	0.000 ± 0.000	0.000 ± 0.000

6.4. Polarization decay in a fill

...

6.5. Spin direction in pC (up-down vs left-right asymmetries)

...

6.6. Final polarizations and uncertainties

...

7. Summary

...

A. Systematic effects studies

A.1. Rate issues

In some parts of Run9 generator pulses with fixed frequency and amplitude injected in the system on the preamp level were used to study and monitor rate effects (usually in bunch 0). The amplitude and ToF (relative to bunch 0) of these pulses were set up in such a way that they do not interfere with C events (banana area) - near 1 MeV in energy equivalent and 70 ns of ToF, as it is shown for example on Fig. 44-top-left. The gen. pulse amplitude in a strip was distributed roughly with $\sigma = 2 - 3$ counts, with larger variation from strip to strip (e.g. in Blue1 in Fig. 44 with $\sigma \sim 8$ counts), wheris ToF variation was small. As it is seen from the comparison of Fig. 44 and 45, in high rate condition we obviously start experiencing problems in measuring both event rate (miscounting them) and amplitude (with supressed gains). ToF doesn't show any obvious signs of distortion. Fig. 46 demonstrates how the gen. pulse amplitude distribution is distorted when target reaches the beam center (maximum carbon event rate).

High rate problems were first detected in previous years, when we accidently put thick target and observed bunch dependent asymmetry - similar to what is shown in Fig. 48
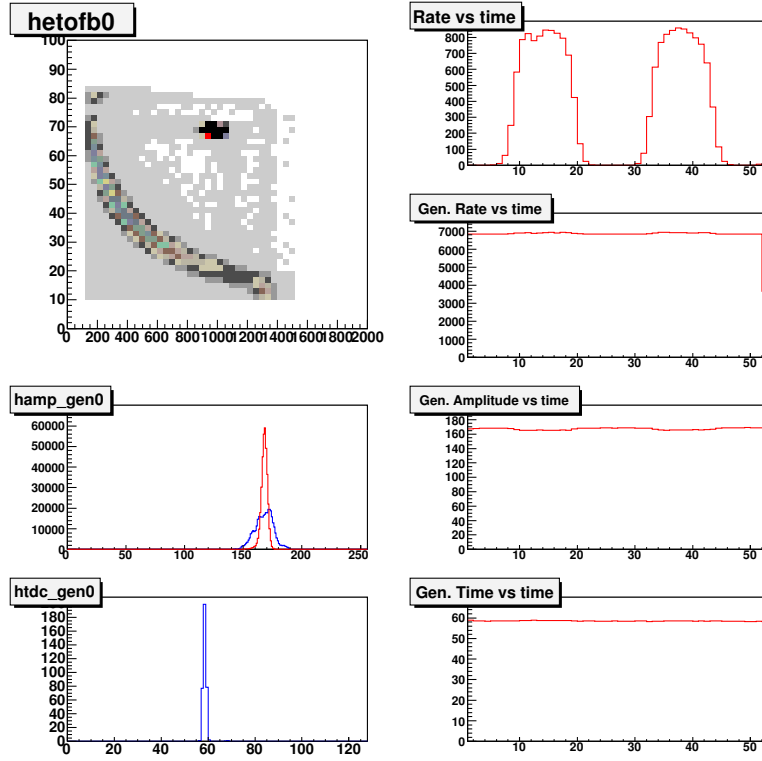
Figure 44. Measurement 10429.013 (Blue1, low rate: 20 kHz/strip), all strips combined. Left-top: ToF (ns) vs deposited energy (keV); "banana" area corresponds to recoile C, activity near (1 MeV, 70 ns) corresponds to injected generator pulses; Left-middle: blue - amplitude distribution (in counts), red - aligned amplitude distribution (peak values of amplitude distributions from gen. pulses aligned in all strips); for the area ToF¿60 ns, ampitude ¿ *** keV. Left-bottom: ToF distribution (in counts); for the area ToF¿60 ns, ampitude ¿ *** keV. Right column plots show time dependence in 1 sec. bins: event rate in the banana, gen. pulse rate, gen. pulse amplitude and gen. pulse time of flight.
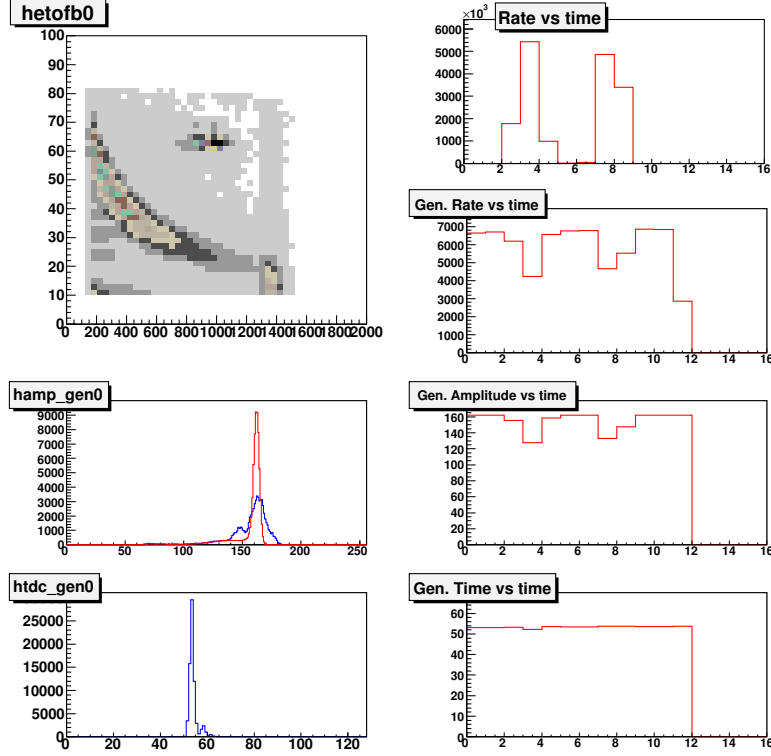
Figure 45. The same as Fig. 44 but for the measurement 10450.116 (Yell1, high rate: 110 kHz/strip).

and 49 (compare to Fig. 47 with no such an effect). Our further tests showed that the difference between up and down bunch asymmetries (distance between red and blue points in Fig. 48 and 49) on the average was not bunch dependent (within stat. errors), which means that detector left-right asymmetry gradually changes with bunch number after the abort gap.

Similar bunch dependence was observed in the reconstructed recoile carbon mass in high rate conditions (compare Fig. 50 and 51), which can come from bunch dependence of either amplitude or time of flight measurements in our system and which can be slightly different in the left-right (or up-down) detectors, and so introducing detector left-right (or up-down) asymmetry.

A.2. Hamamatsu detectors vs BNL detectors

Below we compare the bahavior of Hamamatsu strip and BNL strip detectors installed in Blue2 polarimeter (detectors 1 and 4 and detectors 0,2,3 and 5, correspondingly). We already compared the time dependence of detector response to alpha particles (Fig. 7) and the fill (time) dependence of "Dead layer" and T0 parameters (Fig. 20 and 17). Despite that the amplitude characteristics of two types of detectors are obviously different (the average response to alphas and "Dead Layer"), the time (fill) dependence didn't show any obvious difference, except the energy slope parameter shown in Fig. 52 and 53. It also was reflected in instability of the ratio of beam asymmetry vs fill measurements using 45 degree (BNL) detectors and 90 degree (Hamamatsu) detectors.at $\sqrt{s} = 200$ GeV, as
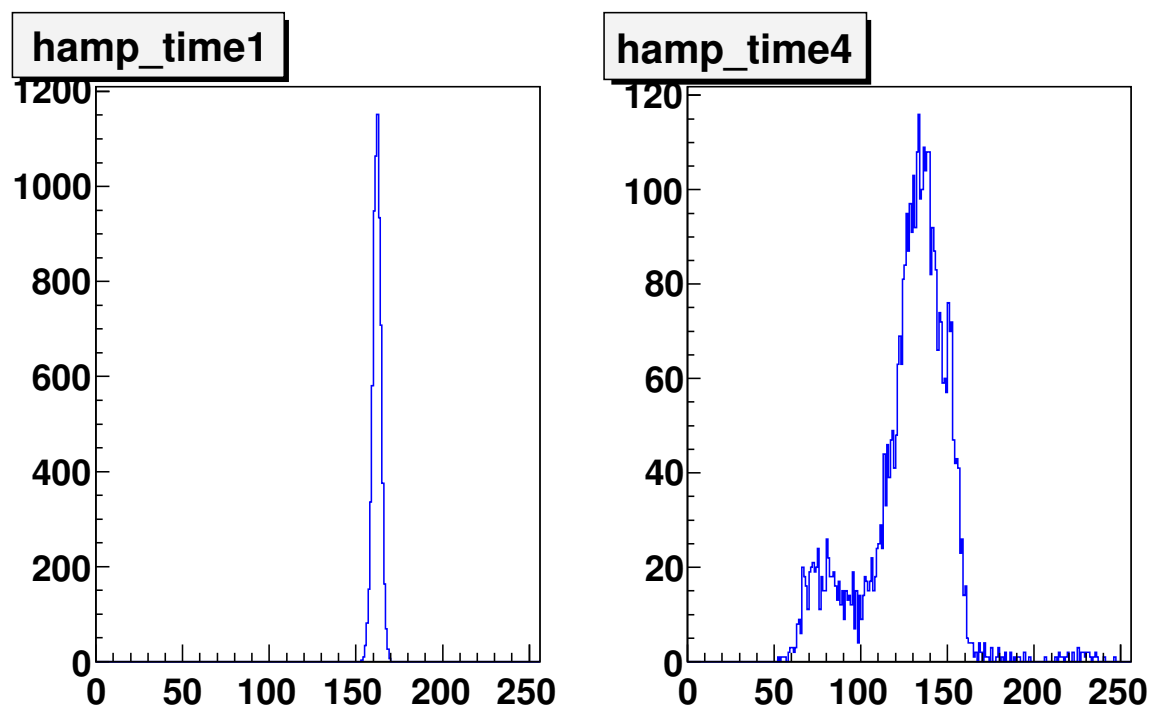
Figure 46. From the measurement on Fig. 45 Gen. pulse amplitude distribuition (all strips combined). Left: target is out of beam (time bin 0-1 sec. on Fig. 45); Right: target at beam center (time bin 3-4 sec. on Fig. 45).
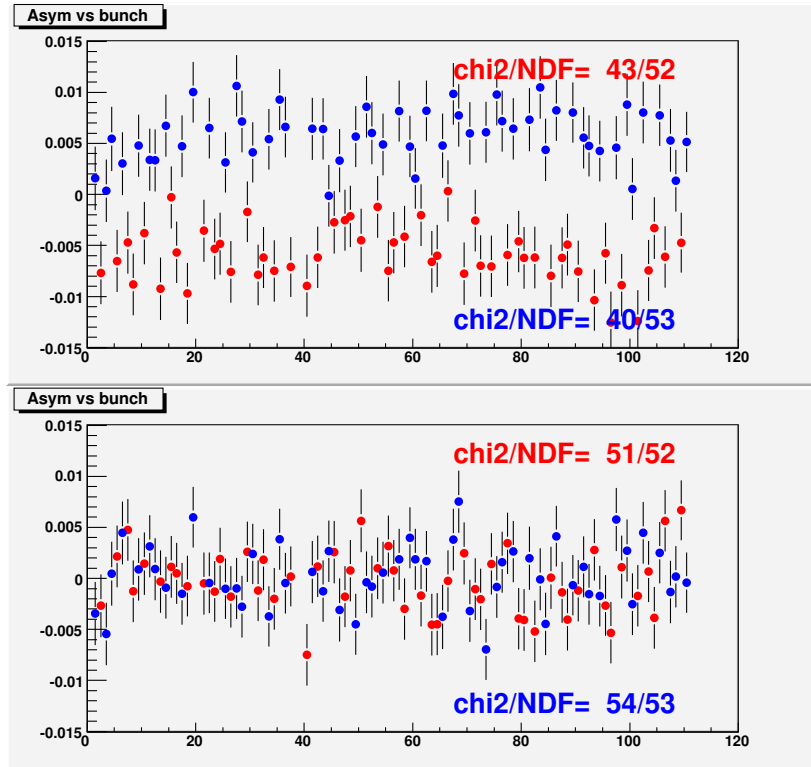
Figure 47. Measurements 10490.005 (Blue1, reasonble rate: 60 kHz/strip): bunch by bunch asymmetry corrected for the average over bunches detector asymmetry; blue points for bunches with spin up, red points for bunches with spin down; top plots for left-right asymmetry, bottom plot for up-down asymmetry (supposed to be near zero).
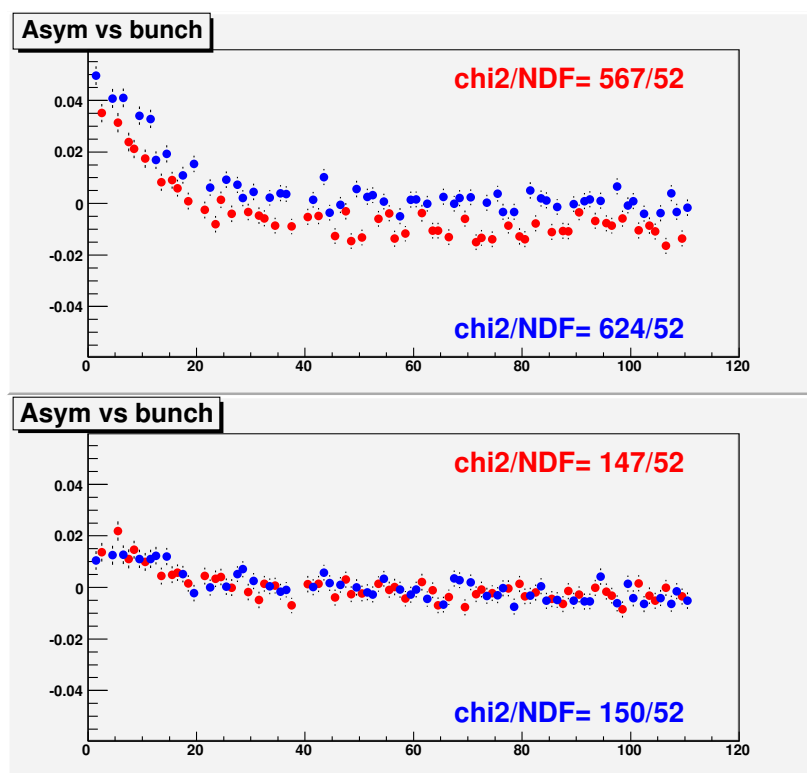
Figure 48. The same as Fig. 47 but for the measurement 10439.008 (Blue1, high rate: 120 kHz/strip).
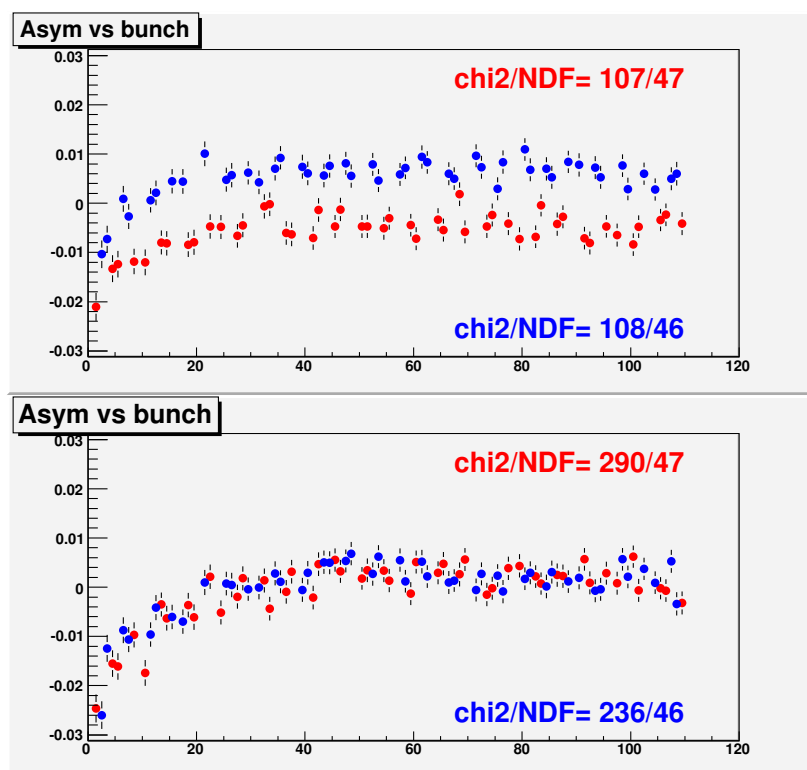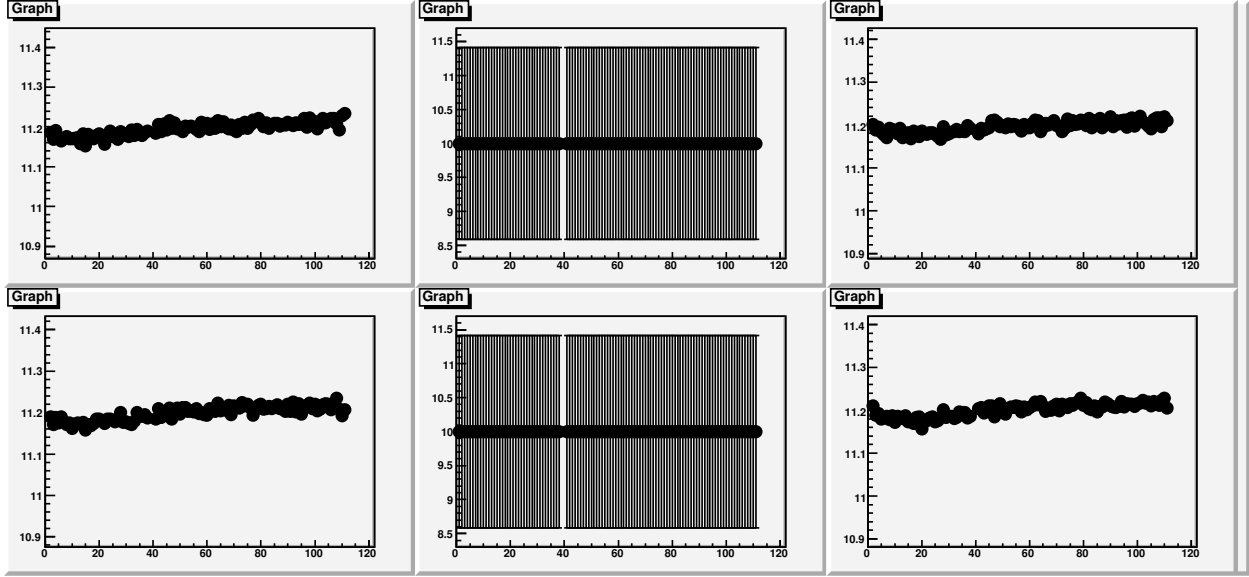

Figure 49. The same as Fig. 47 but for measurements 10402.310 (Yell2).

Figure 50. Measurements 10490.005 (Blue1, reasonble rate: 60 kHz/strip, Reconstructed carbon mass (GeV/c^2) from the measured recoile carbon energy and time of fligh, in detectors 0,1 and 2 (upper row) and 3,4 and 5 (lower row); detectors 1 and 2 (at 90 degree) were off due to horizontal target used for this measurement.
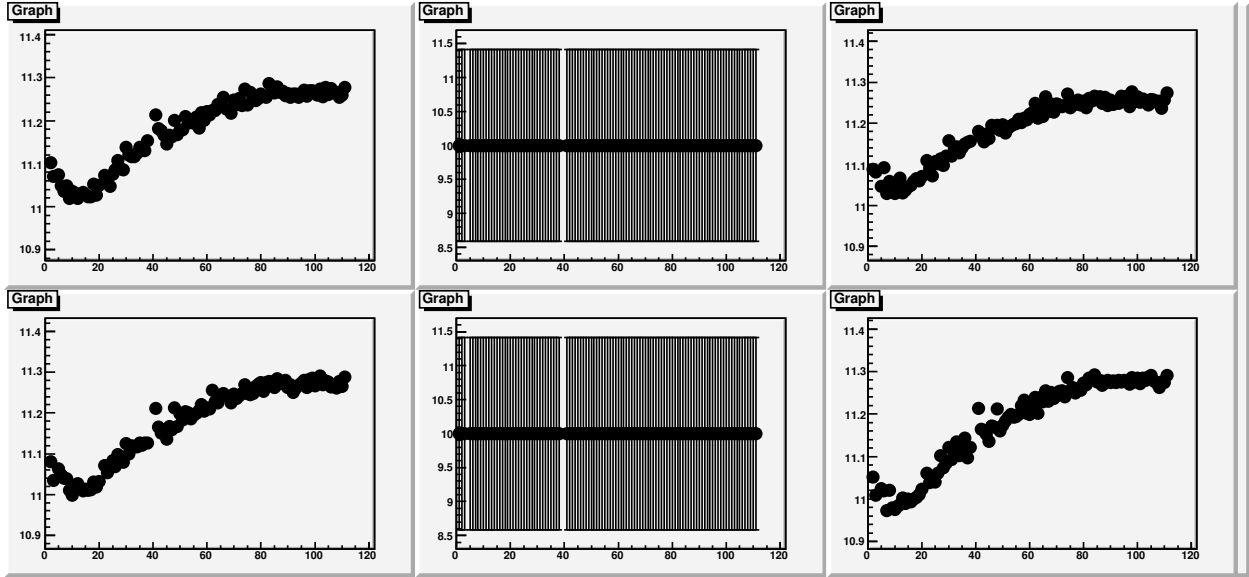

Figure 51. The same as Fig. 50 but for the measurement 10439.008 (Blue1, high rate: 120 kHz/strip).

seen from Fig. 56: e.g the average ratio for fills **-** is **, while for fills **-** the ratio is **. At the same time the instability of energy slope parameter didn't show up in polarizations in $\sqrt{s} = 500$ GeV measurements above stat. errors (Fig. 55). Notice that the expected ratio here is ~ 0.707 ($= \sqrt{2}/2$). Slight discrepancy between this value and observed ratios of ~ 0.68 may come from slight geometrical misalignment of 45 degree detectors and masked strips.

REFERENCES

1. I. Nakagawa, at al, RHIC/CAD Accelerator Physics Note 275, 2007.
2. V. Dharmawardane, at al, RHIC/CAD Accelerator Physics Note 355, 2009.
3. I. Nakagawa, private comminication.
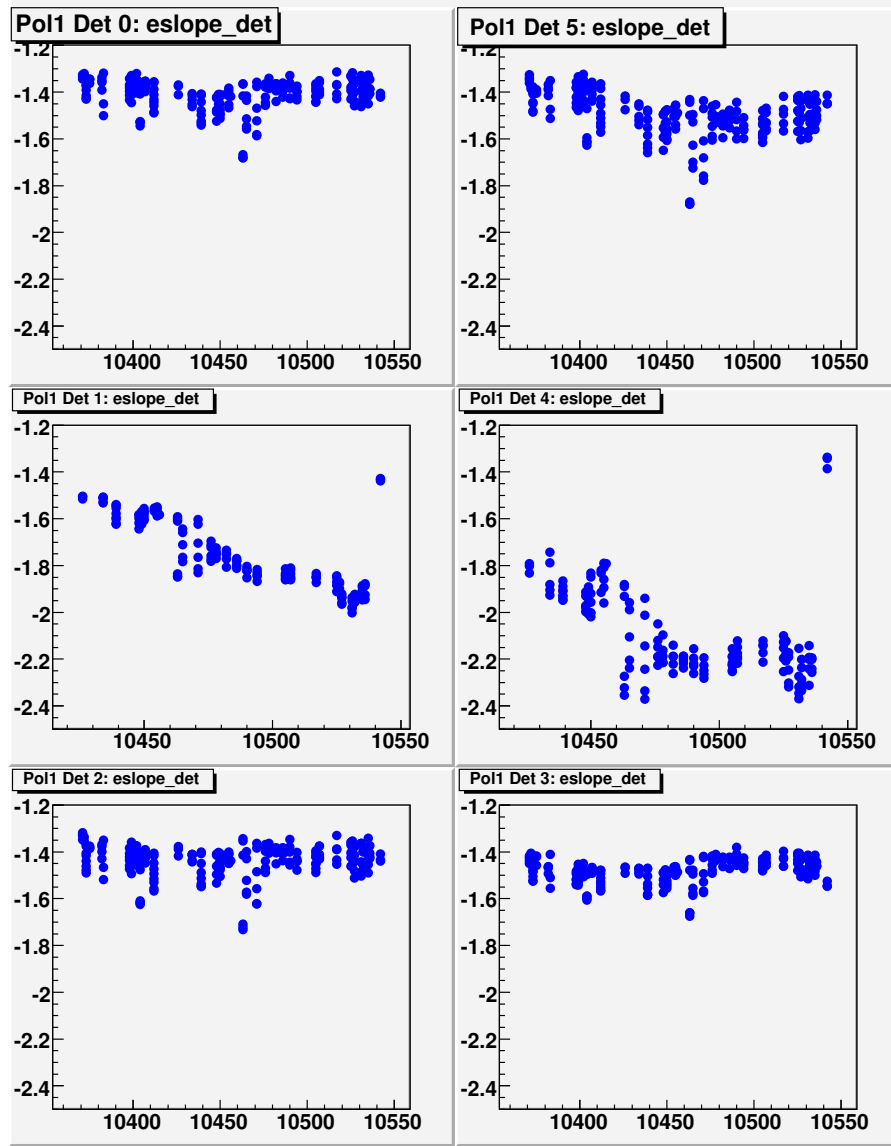4. Haixin, talk at RSC meeting Oct 2 2009.

Figure 52. The average over the detector strips the slope of the fit of dN/dE_{kin} vs E_{kin} to exponent times 10^{-3} in $\sqrt{s}$=500 GeV measurements by Blue2 vs fill number (each fill usually had several measurements, all of them are shown here); all 6 detectors are shown, detectors 1 and 4 (middle plots) being Hamamatsu strip photodiods, all others being BNL's Si detectors; only measurements with vertical target are shown.
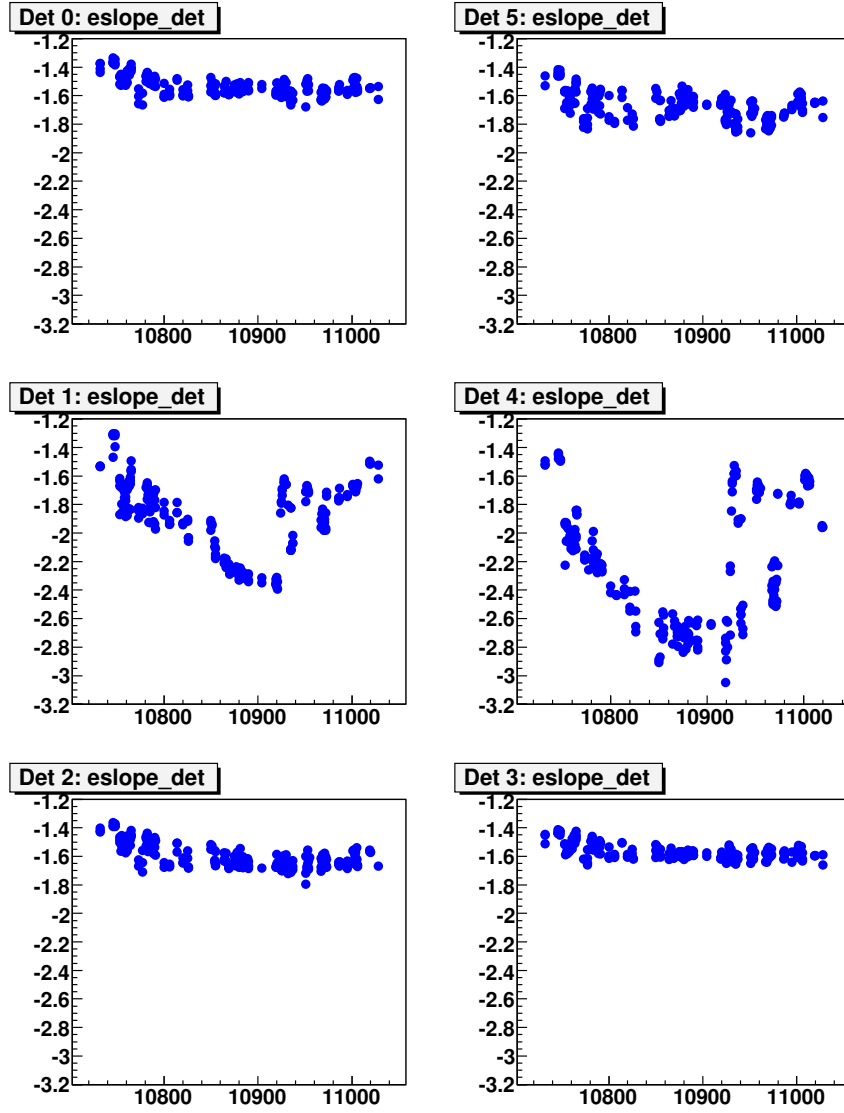
Figure 53. The same as Fig. 52, but for $\sqrt{s}$=200 GeV measurements; notice that Blue1 didn't have measurements in fills >10773.
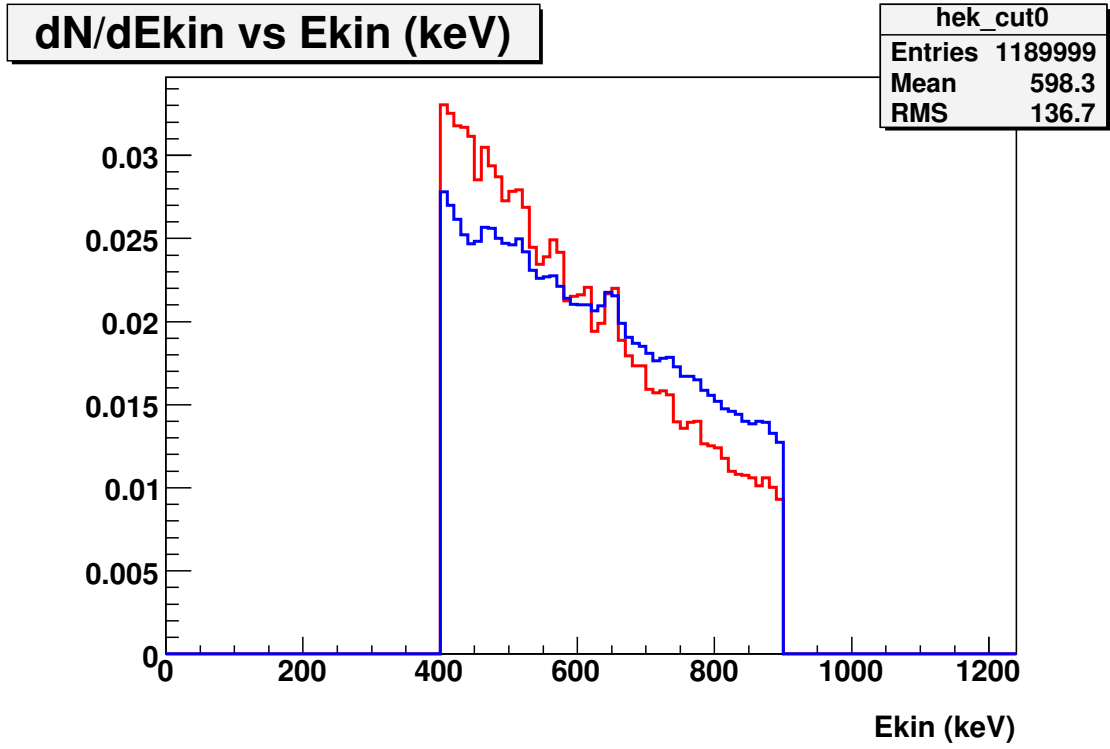
Figure 54. The normalized recoil Carbon kinetic average distributions (dN/dE_{kin} vs E_{kin}) in the E_{kin} range 400-900 keV for the strips in detector 4 (Hamamatsu strip) of Blue2, red for measurement 10746.204, blue for 10854.204; the slope parameters of exp fit are $-1.5 \cdot 10^{-3}$ and $-2.5 \cdot 10^{-3}$ for these two measurements, correspondingly.
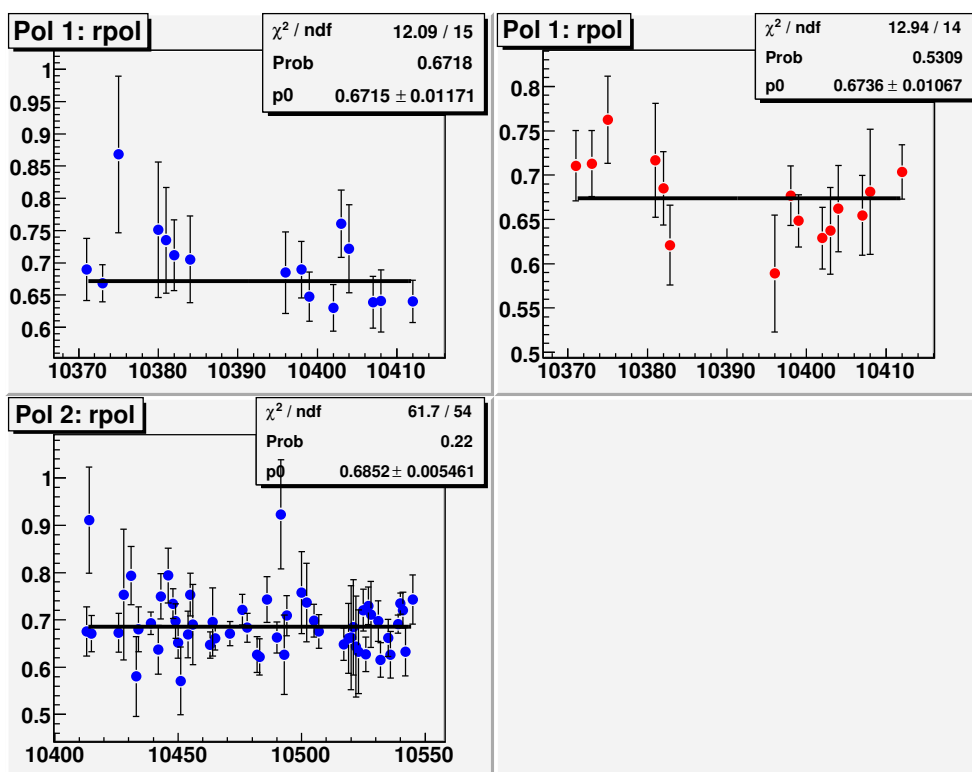
Figure 55. The fill dependence of the ratio of the beam spin asymmetries measured by 45 degree (BNL-type) detectors and 90 degree (Hamamatsu-type in Blue2 and BNL-type in Blue1 and Yell1) detectors; top-left - Blue1, bottom-left - Blue2 and top-right - Yell1 (in Yell2 45 degree detectors were not used.
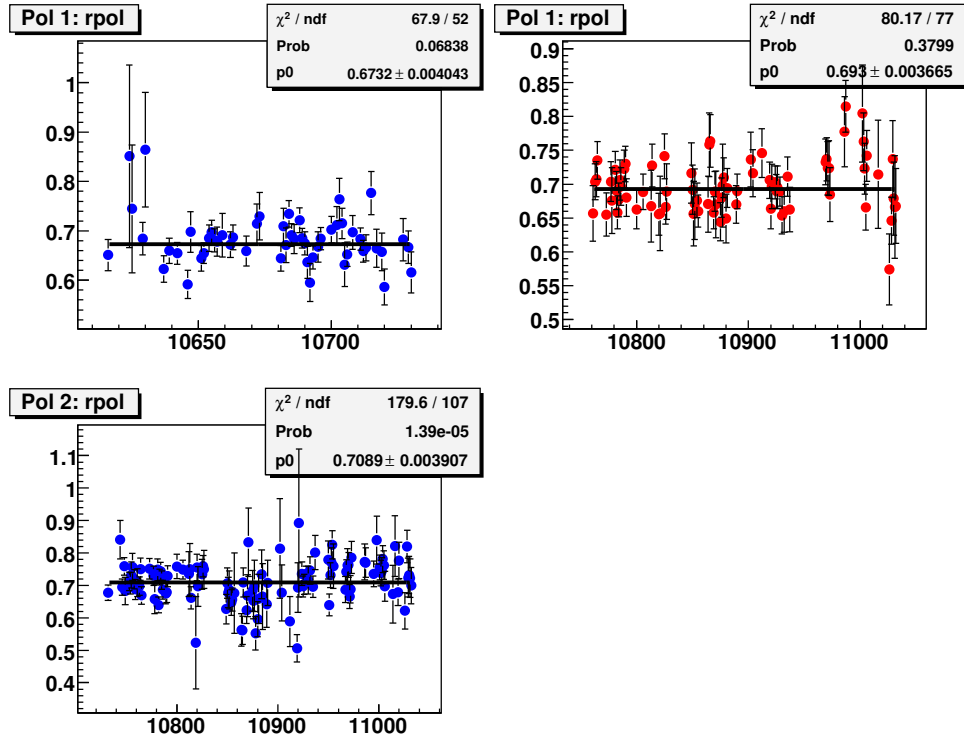
Figure 56. The same as Fig. 55, but for $\sqrt{s}$=200 GeV measurements; notice that Blue1 didn't have measurements in fills >10773.